Unraveling the effect of convergence obliquity on overriding-plate deformation and strain partitioning in subduction zones

Unraveling the effect of convergence obliquity on overriding-plate deformation and strain partitioning in subduction zones

N. G. Cerpa[*,1], S. Lallemand[1] and A. Heuret[2]

[1]*Geosciences Montpellier, University of Montpellier, CNRS, Université des Antilles, Montpellier, FR*

[2]*Université de Guyane, Cayenne,FR*

Corresponding author (e-mail: nestor.cerpa@umontpellier.fr)

Abstract

The subduction of an oceanic plate causes deformation of the overriding plate, from the forearc to the back-arc regions. Over years, to address the physical controls on such a deformation, various compilations on active deformation have been made, mixing various types of datasets including fault-slip rates, focal mechanisms and geodetic motions. The growing amount of available data now allows for the construction of consistent compilations in terms of data types. Here, we present a database for the kinematics of subduction zones which includes that of the overriding-plate deformation, consistently based on geodetic data. The database describes the 2-d (trench-normal and trench-parallel) motions of arc blocks for ~90% of active subduction zones, through the magnitude (v_d) and the deformation-obliquity angle (O_{vd}) between the blocks and the upper plate (undeformed interior of the overriding plate). We classify subduction zones into 4 dominant strain classes (compressional, strike-slip, extensional, and neutral), and into up to 8 classes including intermediate regimes. Focusing on the strike-slip strain class, we show that a non-negligeable trench-parallel motion is a widespread feature of active subduction zones. The convergence obliquity exerts, however, a contrasting effect on O_{vd}, thereby suggesting a limited effect on strain partitioning at oblique subduction zones. On another hand, O_{vd} shows a positive correlation with slab dip, where low and high values are associated with compression and extensional classes, respectively. Finally, we provide revised estimations of subduction rates, allowing for instance refined estimations of the thermal parameter, which will permit future comparative investigations on subduction dynamics and tectonics.

I. Introduction

Subduction dynamics leads to the deformation of the overriding plate which encompasses all tectonic regimes from back-arc spreading to mountain building (Uyeda and Kanamori, 1979). Using geological and geophysical global datasets, various statistical studies have characterized the deformation of the overriding plate for present-day subduction zones, focusing on characterization of one-dimensionnal trench-perpendicular deformation regimes (Doglioni et al., 2007; Heuret & Lallemand, 2005; Jarrard, 1986; Lallemand et al., 2005; Petricca & Carminati, 2016; Schellart, 2008b, 2008a). For instance, arc-to-back arc one-dimensional deformation rates were inferred from geodetic velocities and geological deformation rates by Heuret and Lallemand (2005) and Schellart et al.

(2008b). In addition, focal mechanisms were used to define semi-quantitative overriding-plate strain classes (Jarrard, 1986; Lallemand et al., 2005). These studies showed some correlations of the trench-normal overriding plate deformation to overriding plate motion (Heuret & Lallemand, 2005; Jarrard, 1986), to the slab dip (Lallemand et al., 2005), and to the combination of overriding plate motion and distance to a slab edge (Schellart, 2008a, 2024).

While the global statistical studies listed above focused on deciphering the controls on one-dimensional trench-normal deformation of the overriding plate, in nature, however, deformation is, at least, a two-dimensional process, and the direction of maximum deformation most often deviates from the normal to the trench. This can produce, in extensive settings, for instance, a misorientation between the direction of back-arc spreading and the trench normal. This is the case in the southern Marianas, in the North and South Sandwich back-arc, and most notably in the Andaman Sea. But the most striking observation on the two-dimensionality of overriding-plates deformation is strain partitioning at oblique subduction zones. Oblique subduction zones are those where the convergence vector between the subducting and the overriding plates deviates from the direction of the normal to the trench, and appear as the rule rather than the exception in present-day subduction zones (Jarrard, 1986; Philippon & Corti, 2016). In a pioneering work, Fitch et al. (1972), suggested that oblique convergence was mostly consumed along strike-slip faults quasi-parallel to the trench while the remaining was taken up on thrust structures. Jarrard et al. (1986) later demonstrate that the strike-slip or transcurrent motions tend to increase with the obliquity angle (see also McCaffrey, 1992; Yu et al., 1993), and that they are more frequent at oceanic-continent subduction zones. In many cases, the strike-slip fault (system) that accommodates strain partition, occurs in the vicinity of the arc and defines a “forearc sliver” that tends to move independently of the interior of the overriding plate. Among the most notable examples of strike-slip faults accommodating partition are the Great Sumatran Fault (Bellier & Sébrier, 1995), the Philippine Fault (Barrier et al., 1991), the Southern Kuril strike-slip system (DeMets, 1992; Kimura, 1986), the Chingual-Cosanga-Pallatanga-Puña Fault in the Northern Andes (Alvarado et al., 2016; Baize et al., 2020) or the Yaeyama Fault in the Southern Ryukyus (Lallemand et al., 1999). It is also worth noting that even though strain partitioning originally referred to partition of slip on two localized faults, the term has also been more generally used for any type of deformation partition, whether localized or diffuse, including some component parallel to the subduction trench such as the set of conjugate and transcurrent strike-slip faults in SW Japan (Gutscher & Lallemand, 1999) or the Sorong Fault system in New Guinea (Patria et al., 2021).

Despite a long list of physical studies that investigated the conditions which may or may not allow for strain partitioning, no consensus has yet emerged (Byrne et al., 1985; Chemenda et al., 2000; Cooke et al., 2020; Dominguez et al., 1998; Haq & Davis, 2010; Jarrard, 1986; Liu et al., 1995; Martinez et al., 2002; McCaffrey, 1992; McClay et al., 2004; Suárez et al., 2022). One of the potential limitations to address strain partitioning, and more generally, to address the amount of overriding plate deformation in space and its relation to other subduction processes, has been the lack of a complete global database for present-day subduction zones. This is precisely the purpose of the present study where we have built a database of the direction and intensity of the main sites of overriding plate deformation.

We present a comprehensive update on the kinematics component of the Submap database (Heuret, 2005; Lallemand & Heuret, 2017). The latter database consists in the sampling of all present-day subduction zones approximately every 200 km, amounting to a total of 260 subduction transects, for which a wide range of parameters have been constrained from the compilation of a wide range of published studies. The parameters include data on kinematics (Cerpa et al., 2022b; Heuret & Lallemand, 2005), on the subducting slab geometry (Lallemand et al., 2005), on the structural parameters (Heuret et al., 2012; Lallemand et al., 2024), and on the characteristics of the seismogenic zone (Heuret et al., 2011). In particular, the kinematics in the Submap database compiles information on the absolute and relative plate motions, the subduction rate, and the deformation rate of the overriding plate. This compilation has been widely applied in studies of diverse topics, from subduction dynamics (Faccenna et al., 2007; Funiciello et al., 2008; Lallemand et al., 2008; Nakao et al., 2022) to the seismogenic behavior of the plate interface (Brizzi et al., 2018; Marzocchi et al., 2016; Wirth et al., 2022; Zelst et al., 2025).

Our update concerns the relative and absolute plate motions at subduction trenches, accounting for estimations of the overriding plate deformation rate, following preliminary work in Cerpa et al., (2022b). Importantly, in the previous version of the Submap kinematic database, Heuret and Lallemand (2005) determined only the trench-normal overriding-plate deformation velocity v_{d_n}, providing non-null values of v_{d_n} for about half of the Submap transects. In the current update, based on the most recent literature, we are able to reach a spatial description (full vector v_d) for 78% of the transects. It is also worth noting that information on the overriding-plate deformation rates allows for a more precise estimate of subduction rates at present-day than what would be constrained solely based on the far-field subducting plate and overriding plate velocities obtained from global plate kinematic models (i.e., by the estimation of the convergence rate).

Below, we describe how we built the kinematic database. Then, we assess global characteristics of overriding-plate deformation, before assessing its relationship to other subduction parameters. Finally, we discuss some implications of revised values of the rates of subducting-plate consumption at trench, i. e. the subduction velocities.

II. Building the kinematic database

II.1. General definitions

For describing the kinematics at each subduction transect of the Submap database, we associate each transect to a subducting plate (SP) and to an undeformed area of the overriding plate, which we refer to as the upper plate (UP) (Figure 1). The SP and the UP move at absolute velocities of V_{sub} and V_{up}, respectively. Here, by "absolute velocities" we mean velocities that describe the motion of the plates relative to a deep, stable, reference frame, often taken to be the Earth lower mantle. The sum of these two velocities gives the convergence velocity $v_c = V_{sub} + V_{up}$, that is the rate at which the assumed undeformable interiors of the two plates move relative to each other.

In nature, however, the overriding plate generally undergoes deformation in the forearc, in the arc and/or in the back-arc regions. The deformation may either localize on one or more faults, or being diffuse across part or all of the forearc-to-back-arc regions, sometimes leading to the formation of a sliver which moves semi-independently of the UP. Thus, to account for the overriding-plate deformation, we define a deformation velocity v_d which aims to integrate any deformation occurring from the forearc to the back-arc, whether it is distributed or localized at single faults. In doing so, we define a real or an idealized pseudo-kinematic block, that we refer to as the "arc" block (AB). The velocity of the AB relative to the UP is given by v_d. Knowing the latter, we can assess an absolute trench velocity V_{trench} which differs from V_{up} if $v_d \neq 0$. Finally, we can define the subduction velocity $v_s = V_{sub} + V_{trench}$ which best represents the rate of SP consumption at trench. It is supposed to represent the slip velocity on the subduction interface estimated by geodesy, and which can be compared to the seismic slip velocity inferred from the seismic moment of the earthquakes on the subduction interface (Brune, 1968).

We define the SP and UP for each subduction transect from the major plates of the plate set model MORVEL56 (Argus et al., 2011), which also gives us the convergence velocities between those plates. As described in details below, we assess the deformation velocities in the present-day subduction zones, which also permit us to provide an estimation of the subduction velocity. Moreover, although the present study focuses on relative velocities (v_c, v_s and v_d), we have calculated absolute velocities (V_{sub}, V_{up}, and V_t) for each transect in four selected absolute references frames: MORVEL56-NNR model (Argus et al., 2011), the spreading-alignment model (Becker et al., 2015), the T25m model (Wang et al., 2018), and the GMHRF-1Ma model (Doubrovine et al., 2012). Although not exhaustive, such a selection covers part of the variety of absolute plate kinematic models, e.g., in terms of the data used to establish them (see Cerpa et al., 2022b).

For all type of velocities, we calculate their obliquity *O* relative the normal to the trench. We can then calculate the trench-normal and trench-orthogonal component of all velocities, which are denoted with the subscripts $_n$ and $_t$, respectively.

II.2.Arc blocks and estimation of deformation velocities

We seek to characterize the deformation of overriding plates in relatively close distances to the subduction trenches, by estimating v_d for as many subduction transects as possible. This relies on the definition of an AB for several subduction segments, inferred exclusively from GPS data.

To illustrate how we integrated the deformation of the overriding plate predicted by GPS studies into v_d , we take the example of the South-East Asia region (see Figure 2) which illustrates the several possible definitions of an AB:

- An AB is defined as one of the plates in the MORVEL56 plates set (dark blue patches in Figure 2a and in Table 1), if the latter plate occupies a region which is small relative to the size of the large plates taken to be the upper plates (Eurasia plate, Sunda plate, Philippine Sea plate, etc.). This is, for instance, the case for the Andaman subduction transects for which we take the Sunda plate from MORVEL56 as the UP, and the

Burma plate from MORVEL56 as the AB. This is also the case for the Mariana transects where both the UP and the AB are from the MORVEL56 plates set.

- An AB is taken from a GPS-derived rigid block defined in published studies, with available Euler pole and rotation rate (light blue patches in Figure 2ab and Table 1). Two sub-cases exist here:
    - 1) The AB motion was neglected in the MORVEL56 plate set model. This is, for instance, the case for the Sumatra transects for which the Sunda Plate from MORVEL56 is the UP, and for which we take into account the Sumatra forearc sliver block described by Bradley et al. (2017).
    - 2) An update of the AB motion post-MORVEL56 is available and we thus modify part of a block of the MORVEL56 model. This is the case for the case for the Yonaguni block at the southwestern end of the Ryukyus transects (Chen et al., 2022), which substitutes the southernmost solution given by the Okinawa block of MORVEL56
- In some other cases (Taiwan, Luzon, Visayas and East-Philippines), the UP deformation appears distributed. GPS velocities have been published for specific stations (Hsu et al., in press; e.g. Rangin et al., 1999; Simons et al., 2007; Socquet et al., 2006) but no rigid blocks have been identified in past studies. In such cases, we extract, from published studies, the motion of the station closest to the trench as a proxy of AB motion. We then post-calculate the deformation rate v_d between the forearc and the UP by difference between both GPS velocities, thereby neglecting

the interseismic loading, if any. We refer to these regions as to deformed areas (red patches in Figure 2ac and Table 1).

- In regions such as the Southernmost Marianas or the Northernmost Philippines, we did not find any published geodetic-velocity solution for the overriding plate deformation despite geological evidences of recent deformation (Hsu et al., in press; Ribeiro et al., 2013). For those cases, we set v_d as undefined (rather than 0). However, we make use of the a MORVEL-56 derived solution for v_c and assume that $v_s = v_c$ (blue stripes in Figure2a and Table 2).
- Finally, in Halmahera, Sangihe, South Philippines or Sulu, the use of M56 plate kinematics provides unreasonable values of v_c because UP or SP are difficult to constrain. Despite the scarcity of GPS data in those regions, we utilized the published motions of a few stations on both sides of the trench to provide first-order estimates of v_s, but not to retrieve v_d. We define these cases as the deformed areas (red stripes in Figure2a and Table 2).

Exceptionally, and for reasons of consistency, we have assigned a v_s extrapolated from adjacent transects on one of our transects across the Manila Trough because at this latitude only the Philippine Sea plate (UP) motion relative to the Sunda plate is known through the GPS stations installed on the Batan islets despite the fact that the forearc deforms (Martinez et al., 2002).

In addition to the above exposed cases, there are further specificities which are not encountered in the Southeast-Asia region but which are to be noted for a few transects in other regions:

- For NE Japan subduction transects (Figure 3), the Okhotsk plate from MORVEL56 is taken to be the AB while the Amur Plate is taken to be the UP. Further north, for the northern Kurils and for the Kamchatka transects, the Okhotsk plate is rather defined as the UP. Only for the South-Kuril transects, we are able to provide a solution for the motion of a pseudo-rigid AB. For the other transects in this area we have not defined an AB (though the UP may be experiencing active deformation, see below).
- For the northernmost Andean transects, the AB motion was taken from (Jarrin et al., 2023) in place of the entire north Andean block of MORVEL56.

Overall, this inventory leads to the use of 11 ABs from the M56 plates set, 35 additional rigid ABs and 14 additional pseudo-ABs or deformed areas for which v_d are indirectly constrained by single GPS stations (Table 1). Furthermore, we also have identified 13 regions where v_d is not constrained (Table 2), but 4 of them for which v_s can be derived from GPS and 9 for which we assume v_s = v_c. The 73 areas are displayed in Figure 3. The names of the blocks together with the references from which they were taken, are listed in Table 1 and 2.

II.3. Potential limitations of our approach

Our estimation of the deformation vector v_d is exclusively based on geodetic data and most often derived from rigid blocks. While in most cases the use of these blocks improves the estimation of relative subduction velocities, the rigid solution near extremities of the slivers may be poorly resolved in some cases. We thus preferred to ignore, for instance, the AB corresponding to the western termination of the Scotia plate at the southernmost tip of Patagonia, as the Eulerian solution of its motion relative to the South America plate did not match the deformation observed in the field (Perucca et al., 2016). Furthermore, the deformation of the submerged forearc or backarc may be underestimated because of the lack of ocean bottom geodetic stations.

In a few regions (blue stripes in Figure3), geodetic deformation velocities are unavailable while geological evidence of active deformation exist. These regions include the Kamchatka region which has undergone Quaternary extension at a geological rate of 17 +/- 3 mm/yr (Kozhurin et al., 2006; Kozhurin & Zelenin, 2017), the Central Chile with evidences of Plio-Quaternary compression through tectonic inversion of former extensional faults (Becerra et al., 2013), the Southernmost Patagonia where the forearc consists of the western end of the Scotia plate sliding along the Magallanes-Fagnano left-lateral fault system at a rate of 8.1 +/- 1.5 mm/yr (Perucca et al., 2016), some poorly constrained subduction zones of Southeast Asia including the Banda Sea (Aru, Seram), the Molucca Sea (Halmahera, Sangihe, S- and N-Philippines), and the Celebes Sea (Cotobato, Sulu), the Southermost Mariana arc and forearc undergoing trench-parallel extension (Ribeiro et al., 2013), the Solomon arc which is shortened by subduction-collision of the Ontong-Java plateau (Mann & Taira, 2004), the Southermost New-Hebrides where the arc rotates clockwise as a result of its indentation by the Loyalty Arc (Patriat et al., 2015), as well as the Puysegur Ridge hosting the right-lateral transcurrent Puysegur Fault (Collot et al., 1995). We acknowledge the limitation of the available data for constraining geodetic deformation by marking those regions as undefined rather than marking them as neutral. Moreover, in some cases, we find that it is not even possible to characterize v_c because the complexity of region, including high UP or SP deformation such as that in the Molucca Sea area (Rangin et al., (1999), red stripes in Figure 3). All the above regions where v_d is unconstrained are listed in Table 2. We further split those regions depending on whether v_s is constrained but v_c is not (red stripes in Table 2) or whether we have approximated v_s as v_c = v_s (blue stripes in Table 2).

III. Upper-plate deformation: general characteristics and comparison to geological constraints

III.1. Defining strain classes from the obliquity of the deformation velocity

To analyze globally the kinematics of overriding-plates deformation in the arc to back-arc regions, we seek to define strain classes (e.g., Lallemand et al., 2005). We conduct the classification using the value of the obliquity O_{v_d} of the overriding plate deformation velocity, that is the misorientation of v_d relative to the trench-normal which takes values between 0 and 180° (see Figure 1), or equivalently, on the basis of the directed obliquity $\bar{O}_{v_d}$ which takes values between -180° and 180° (positive for right-lateral and negative for left-lateral components of sliver motions). The reasoning behind our choice, is based on the fact that, within our framework, the ideal cases of pure overriding plate compression, extension and ideal strike-slip, would correspond to values of O_{v_d} equal to 0°, 180°, and 90°, respectively (see Figure 1).

However, the direction of overriding plate deformation generally deviates from these three ideal cases and thus we can expand the definition to define three dominant-strain classes as (see Figure 4a):

- overriding plates undergoing dominant compression are defined when $O_{v_d} < 45°$ (or -45° $< \bar{O}_{v_d} < 45°$)
- overriding plates undergoing dominant extension are defined when $135° \leq O_{v_d} \leq 180°$ (or 135 $\leq \bar{O}_{v_d} \leq 180°$ & -180 $\leq \bar{O}_{v_d} \leq -135°$)

- overriding plates undergoing dominant strike-slip are defined when $45° \leq O_{v_d} < 135°$ (or $45 \leq \bar{O}_{v_d} < 135°\& -135 < \bar{O}_{v_d} \leq -45°$

These three dominant classes can be further declined into seven strain (sub)classes composed of three pure-strain classes (C, E, SS) and four other combinations of these end-members (C-SS, SS-C, E-SS, and SS-E), as illustrated on Figure 4a. We emphasize that, below, we will use the term "dominant compression" to describe collectively the subclasses C and C-SS, "dominant strike-slip" for SS-C, SS, and SS-E, and "dominant extension" for E and E-SS.

It is worth noting that some necessary simplifications underlie our approach to derive strain (sub)classes based on the value of O_{v_d}. In particular, our dominant compressive and extensive regimes are good descriptors of (quasi-)trench normal compression and extension. Quasi-trench parallel compression or extension, would instead fall into our SS classes. Likewise, our strike-slip class is well suited to characterize quasi-trench parallel strike-slip deformation, while oblique to trench-normal strike-slip systems would lie in our C or E classes. However, we argue that these concern only a few cases and that the advantage of our classification is that it permits to carry a consistent global analysis.

With the above caveats in mind, Figures 4b-f provide a global view of the overriding-plate deformation calculated for most of the transects of our database, as well as their associated strain classes. A more synthetic and schematic global overview is provided in Figure 5 along with a piechart of their relative and absolute distribution. In the database, among the 213 transects with constrained non-zeros values of v_d (82% of all transects), we count 40 (19% of all transects), 39 (18% of all transects), and 134 (60% of all transects) transects belonging to the three classes: dominant compression (C, C-SS), dominant extension (E, E-SS) and dominant strike-slip (SS, SS-C, SS-E), respectively. We note that our database describes the deformation of the overriding plates within a mean distance of ~340 km, with a minimum of ~100 km (in eastern Philippines) and up to a maximum of 900 km (in the Altiplano region).

Transects in the pure compression (C, |$\bar{O}_{v_d}$ |< 10°) or pure extension (E, |$\bar{O}_{v_d}$|≥ 170°) regimes are relatively rare (each representing only 3% of all of our transects). The few transects having a pure C regime are in E-Makran (Reilinger et al., 2006), E-Alaska (Elliott & Freymueller, 2020) and C-Andes (Altiplano, Argus et al., (2011)). The transects under pure E regime are found in C-Ryukyus (Argus et al., 2011), the C-Sandwich (Argus et al., 2011), in W-Mexico (Andreani et al., 2008; Selvans et al., 2011) and in N-Marianas (Argus et al., 2011). Compression associated with strike-slip (C-SS, 10°≤|O v_d |<45°) as well as extension associated with strike-slip (E-SS, 135°≤|Ov_d|<170°) represent 13 and 12% of the transects, respectively. C-SS regime is observed along the Andes in Ecuador (Jarrin et al., 2023) and in C-Chile (Brooks et al., 2003), in Timor and Flores (Koulali et al., 2016), in W-Makran (Reilinger et al., 2006), or in C-New Hebrides due to the subduction of the D'Entrecastaux Ridge (Bergeot et al., 2009). E-SS regime is observed in Calabrian (Serpelloni et al., 2007) and the Hellenic area (Vernant et al., 2014), in the Tonga-Kermadec (Argus et al., 2011) and in some portions of the Izu-Bonin-Mariana (Argus et al., 2011; Nishimura, 2011), in C-Aleutians (Elliott & Freymueller, 2020) and in New Britain (Argus et al., 2011).

A pure strike-slip regime (SS, |Ov_d|= 90 ± 10°) is observed in 14% of the subduction zone transects including in the Sumatra (Bradley et al., 2017), the S-Kurils (DeMets, 1992) trenches, in Cascadia (Mazzotti et al., 2002, 2003), in Smost-Chile (Wang et al., 2007), and along some transects of the W- and the E-Aleutians trenches (Cross & Freymueller, 2008; Elliott & Freymueller, 2020). In a higher number of cases though, the lateral component of the deformation is combined with either compression (23% of transects, SS-C, 10° ≤|Ov_d|< 45°) or extension (15% of transects, SS-E, 100° ≤|Ov_d|< 135°). Typical cases of the SS-C regime are in the Andes (Brooks et al., 2003; Jarrin et al., 2023; Villegas-Lanza et al., 2016), in the W-Aleutians and in W-Alaska (Cross & Freymueller, 2008; Elliott & Freymueller, 2020), in Japan (Argus et al., 2011; Nishimura et al., 2018), in C-Philippines (Rangin et al., 1999), in W-Java (Koulali et al., 2017), and on the Muertos Trough (Calais et al., 2022). Examples of SS-E strain regime are observed in C-America (Andreani et al., 2008; Carvajal-Soto et al., 2020), in Andaman (Argus et al., 2011), in the Aleutians (Cross & Freymueller, 2008; Elliott & Freymueller, 2020), and in the Izu-Bonin-Mariana (Argus et al., 2011; Nishimura, 2011) and of Hikurangi (Argus et al., 2011).

We have further classified 6% of our transects as neutral (v_d=0). Typically, the Lesser Antilles falls into this category as it does not how significant upper plate deformation (Symithe et al., 2015).

Finally, we have 30 transects (12% of the total) which we classify as “undefined” since geological observations suggest active tectonics but no geodetic-based quantification of it has been proposed (see Section II.3).

In what follows, although we classified our transects into 8 subclasses of strain regimes (and one “undefined” subclass) we will carry our analysis describing them only in terms of the three classes of dominant regime (cf. Figure 4a).

III.2. Global trends of UP-deformation velocities

The mean of all magnitudes of v_d is ~23 mm/yr but the distribution of the magnitudes shows important differences depending on the dominant strain class (Figure 6a). The mean v_d for both the regimes of dominant compression and strike-slip regimes are around 20 mm/yr, while dominant-extensive settings rise a mean v_d of about 40 mm/yr. As expected, the highest magnitudes (> 80 mm/yr) of overriding-plate deformation rates are found exclusively for regimes of dominant extension. These highest v_d are predicted for fast-spreading centers at the back-arc of Tonga and New Britain subduction zones. More moderate extensive deformation rates (40-80 mm/yr) are observed for the Kermadec, the Ryukyus and the Marianas back-arcs. On the contrary, overriding plates under dominant compression experience mostly deformation rates of less than 50 mm/yr, with 75% of compressive transects deforming at less than approximately 30 mm/yr. Some anomalous high deformation rates are found for the South-Philippines transects, reflecting both strike-slip at the Philippine fault and the presence of retro-subduction zones (Cotobato, Sulu/Negros SZs), and at the site of the collision between the D'Entrecasteaux Ridge and the New Hebrides subduction trench. The transects with overriding plate under dominant strike-slip regime, also show mostly deformation rates of less than ~50 mm/yr. The highest value (81 mm/yr) is predicted for one C-Philippine transects for the reason explained above. Other moderately high values of deformation in strike-slip systems (50-60 mm/yr) come from oblique-spreading settings (Andaman, S-Sandwich, S-Marianas).

To further analyze the deformation rates, we can decompose the rate v_d into a trench-normal component v_{d_n} and a trench-parallel/tangential component v_{d_t} (Figure 1). Our definition of the trench-normal component v_{d_n} is such that overriding plates under dominant compression yield positive values of v_{d_n}, while those under dominant extension rise negative values. The transects with overriding plates under dominant strike-slip motion can be associated with either positive or negative values of v_{d_n}, depicting either overall transpressional or transtentional regimes, respectively. In addition, the trench-parallel component v_{d_t} is also signed with positive values indicating right-lateral strike slip, and negative values left-lateral strike slip (Figure6c).

Figure 6b shows that the absolute values of trench-normal components $|v_{d_n}|$ are less than 60 mm/yr (mean of 17 mm/yr) with a very few transects under dominant extension experiencing higher rates of extension. The values of $|v_{d_n}|$ are generally higher for extensive regions than those of the compressive regions, as noted for the magnitude of the deformation vector. The transects falling under our dominant strike-slip class display values of $|v_{d_n}|$ with a relatively low mean of ~6 mm/yr. Transtention and transpression are almost equally represented by all subduction transects. Figure 6c shows that the absolute value of trench-parallel component $|v_{d_t}|$ for systems under dominant strike-slip can be as high as 60 mm/yr, with a mean value of ~20 mm/yr. Within our classification framework there are more right-lateral strike slip systems (~2/3) than left-lateral (~1/3).

III.3. Relationship between the deformation velocity v_d and the convergence velocity v_c

III.3.1. Degree of strain partitioning

The trench-parallel component of deformation in subduction zones is thought to be promoted by the obliquity of the convergence between SP and UP (e.g. Jarrard et al., 1986; McCaffrey et al., 1992). Before re-assessing this relationship based on our estimations of deformation in overriding plates, we first provide an overview on how the convergence and the deformation velocities compare in terms of their normal and tangential components, by calculating the ratios $\frac{|v_{d_n}|}{|v_{c_n}|}$ and $\frac{|v_{d_t}|}{|v_{c_t}|}$, respectively. Note that the latter has been often referred to as the partition coefficient, and has served to evaluate the efficiency of strain partitioning at oblique subduction zones in which the strike-slip motion was accommodated along a single transform fault (e.g. Chemenda et al., 2000). Hereafter, we refer the ratios $p_n = \frac{|v_{d_n}|}{|v_{c_n}|}$ and $p_t = \frac{|v_{d_t}|}{|v_{c_t}|}$, to as the normal and the lateral partition coefficients, respectively.

The first striking observation for the normal partition coefficient (Figure 7a) is that only extensive deformation velocities can exceed the trench-normal component of convergence. This is most notably the case for the Sandwich ($p_n \approx 7-8$), the New Britain ($p_n \approx 8 - 13$) and the W-Aegean (p_n up to 10) transects, where the trench-normal convergence component mostly remains under 10 mm/yr while the trench-normal component of extension rate is higher than 30 mm/yr, reaching 110 mm/yr in the New Britain. The normal partition coefficient p_n for compressive transects mostly display values of less than 0.6 (75 % of transect). The highest values (0.6 to 1) of p_n in compressive settings correspond to regions where a retro-subduction zone develops (Panama, Tanimbar, Timor, Flores, Philippines) or where subduction of a prominent buoyant feature tends to create a collisional context (Alaska, New Hebrides).

Figure 7b shows the lateral partition coefficient for transects falling within our dominant strike-slip class. More than 75% of those transects have lateral partition coefficient p_t of less than 0.9. Those which have a trench-parallel overriding plate deformation velocity largely exceeding the trench-parallel convergence velocity ($p_t \gtrsim 5$) include those portions of subduction zones experiencing spreading in a direction that depart from the normal to the trench due to trench curvature. The latter cases include the Smost -Marianas ($p_t \approx 8$), the Sandwich ($p_t \approx 7-8$), the C-New Hebrides ($p_t \approx 8$) and Wmost-Aegean ($p_t \approx 5$). Those large values of p_t are also found in regions with oblique retro-arc subduction zones such as Manila ($p_t \approx 9$) and Emost Java ($p_t \approx 6$). Other transects having a high lateral partition coefficient ($p_t \approx 1-5$) include the Nmost Tonga ($p_t \approx 4$), C-Java and W-Java ($p_t \approx 1-1.5$), N-Sumatra and Andaman ($p_t \approx 1.5-2$), as well as the Mexican subduction trench ($p_t \approx 1-5$).

III.3.2. Relationship between the directed O_{vc} and O_{vd}

Figure 8 shows that 84% of the transects undergoing overriding-plate deformation display deformation obliquities O_{vd} that are compatible with the obliquity of the convergence O_{vc}, regardless of the tectonic regime. Seven transects under the strike-slip dominant regime exhibit values $[O_{vc}]$ > 90° which, in the absence of deformation within the arc block, would represent eduction rather than subduction. These 7 transects are all located in five regions (Venezuela, N-Andaman, W-Aegean, E-Tanimbar, Panama) and correspond to subduction zone terminations where the trench azimuth becomes subparallel to v_c and where lateral displacement of AB re-establishes convergence between AB and SP. There are 16% of the transects which fall into the upper-left or lower-right shaded quadrants, where the obliquities have opposite signs. They generally correspond to collisional areas (Wetar, Timor, New-Hebrides, Makran, Solomons, Alaska) or regions characterized by active back-arc extension (Calabria, Aegean, N-Tonga, S-

Sandwich, Ryukyus, Mariana). Extrusion processes and backarc rifting caused by buoyant features indentation can provide an explanation for these "outliers" (Wallace et al., 2005, 2009).

III.3.3. Focus on the strike-slip dominant-strain regime

Next, we focus on the transects which fall in our dominant strike-slip regime ($45° < |O_{v_d}| < 135°$, cf. Figure 4a) to specifically assess the potential relationship between the kinematics of overriding plate deformation and that of the convergence, as proposed by numerous previous studies (e.g., Jarrard, 1986; McCaffrey 1992). These theoretical and modeling works suggested that the obliquity of convergence should transmit a shear force on the plate interface with some lateral component, potentially resulting on lateral deformation in the overriding plate.

As noted above, the transects under dominant strike-slip regime on Figure 8 show that the majority of transects have deformation obliquities that are higher than the convergence obliquity which is consistent with the fact that in most cases the subduction obliquity is lower than that of the convergence. We note, however, a few exceptions for transects in which the convergence is almost tangential to the trench in the presence of a very curved trench such as in the Wmost-Aleutians and Emost-Venezuela. Overall, there is no clear relationship between the obliquity of deformation and that of the convergence. In particular, relatively low convergence obliquities (<30°) are associated with a variety of deformation obliquities within the range 45-135°.

Figure 9 displays the tangential deformation velocity against the tangential convergence velocity. We first note that a few regions (less than 10%) display values of v_{d_t} and v_{c_t} with opposite sign. These cases correspond to trench edges with sharp azimuthal trend changes, often associated with backarc spreading. We then perform an extraction of the transects where deformation is most likely strain partitioning, that is a conversion of part of the convergence velocity into a deformation velocity. In our interpretation, this is given by values of p_t equal or less than 1 (non-transparent green dots). Through the extraction, it clearly appears that $|v_{d_t}|$ increases with $|v_{c_t}|$, which we think is a piece of evidence of a relationship between the convergence and deformation.

Next, following the proposal by earlier studies, we tested the relationship between convergence obliquity Ov_c and the degree of lateral partitioning on the overriding plate p_t, for transects under dominant strike-slip and with $p_t \leq 1$ and $v_d \geq 1$ mm/yr (Figure 10). Again, the criterion $p_t \leq 1$ is, in our interpretation, aims to select the areas where convergence-related strain partitioning may be at play. The criterion $v_d \geq 1$ mm/yr is meant to avoid selection bias of very small deformation-rates which may not be due to convergence. The first-order observation on Figure 10 is that the degree of lateral partitioning is highly variable and that there is no obvious trend appearing between p_t and Ov_c, even when excluding the few cases of high p_t for very low Ov_c or very low p_t for high Ov_c. More in-depth analysis of Figure 10 shows that most of the regions displaying convergence obliquities Ov_c > 25° (S-Kurils, N-Hikurangi, W-Aleutians, Luzon, Sumatra, Nankai, Philippines, Muertos-Hispaniola, Venezuela, N-Colombia, Andaman) are characterized by a forearc sliver migrating laterally along a transcurrent fault. Such a transcurrent faulting occurs even at small values of Ov_c, such as in the southern Chile just north of the triple junction along the Liquine-Ofqui Fault Zone. On the other hand, a number of overriding plates do not localize the lateral component of the deformation onto strike-slip faults, even with high convergence obliquities like Panama, Cascades or Central Aleutians.

Interestingly, analog sandbox models demonstrated that oblique subducting ridges or seamounts favored strain partitioning at the rear of accretionary wedges (Dominguez et al., 1998; Lewis et al., 2004; Martinez et al., 2002). We have thus checked whether the transects displayed on Figure 10 are associated with the subduction of buoyant features. We found that about two third of the displayed transects are indeed associated with prominent buoyant features including the Carnegie Ridge, Cocos Ridge, Hikurangi Plateau, Palawan Ridge, Benham Plateau, Bahamas bank, Caribbean Plateau, Taiwan Coastal Range, Gagua Ridge, Izu-Bonin Arc, Palau-Kyushu Ridge, Obruchev Rise, and Papuan Peninsula. Our exercice allows us to confirm that most of the transects which exhibit a high degree of partitioning are on or close to a prominent subducting high.

IV. Implications of our new kinematic database

IV.1. Comparison to previous studies

Based on previous compilations of overriding plate deformation at present-day subduction zones, several correlations have been highlighted. Here, we re-assess and discuss some of those correlations based on our determination of the sub-actual deformation of upper plates.

IV.1.1. Overriding plate strain and slab dip

Lallemand et al., (2005) classified 159 subduction transects within three discrete-strain classes (neutral, compressive, extensive) based on a qualitative assessment of focal mechanisms in the back-arc of the overriding plate. Moreover, based on Wadati-Benioff zones, they defined a shallow slab dip α_s representative of a mean subduction angle between the surface and a 125-km depth, and a deep slab dip α_d more representative of the subduction angle beyond a 125-km depth. The authors suggested a direct relationship between the slab dip and the overriding plate strain. Compressive transects were found for deep slab dip lower than 30° while extensive transects were mostly observed for deep-slab dip values higher than 50°.

To revise the correlations, we have re-computed the shallow and the deep slab dips, using the Slab2.0 model (Hayes et al., 2018), when available. To keep consistency with past works, we have adopted similar definitions. For each subduction transect, the shallow slab dip α_s is computed by averaging the estimated dip between 10 and 125-km depths. The deep slab dip α_d is the average dip between 125 and 400-km depth.

We assume that our quantification of the obliquity of the deformation velocity provides a continuous description of the overriding-plate strain (see section III.1) and allows for the application of a linear regression analysis with slab dip. Taking all of our 213 subduction transects with a defined value of v_d, we find weak correlations between the obliquity of deformation and both the shallow (Figure 11a) and the deep (Figure 11b) slab dip. However, excluding complex areas such as the Southeast Asia (Taiwan, Philippines, Banda Sea region, Molucca Sea region, etc), the Mediterranean and the Melanesia, we find a good correlation (linear correlation coefficient $r = 0.58$, Figure 11c) between the shallow slab dip and the obliquity of deformation for the 160 transects. A few large subduction trenches, such as the Alaska-Aleutians from east to west, the Andaman-Sumatra-Java from south to north, and Izu-Bonin-Marianas, illustrate the tendency of deformation obliquity to increase with the shallow slab dip. On one hand, the transects of subduction zones that fall in the compressive class (Andean, Alaska) generally exhibit values of α_s between 10° and 20°. A few outliers in Central America (Costa Rica) and Southern Japan (Kyushu) are compressive but display higher values of shallow slap dip. Those outliers may be explained by the subduction of shallow bathymetric features: the Cocos ridge and the Kyushu-Palau ridge as well as the Amami-Daito-Oki-Daito massif, respectively, which may enforce compression locally but do not lead to significant flattening of the subducting plate (Gardner et al., 2013; Lallemand, 2016). On the other hand, the transects of subduction zones that fall in the extensive class most often exhibit values of α_s higher than 25°. Note that a few transects belonging to the Nmost and Smost-Sandwich subduction trench lie in our strike-slip class but this is biased by the orientation of the subduction transects relative to the direction of back-arc spreading.

Contrary to the findings of Lallemand et al., 2005, our database suggests only a weak correlation between the deep slab dip and the deformation obliquity, regardless of the

exclusion of complex areas (see Figure 11d). Although some tendency to increase Ov_d with α_d is perceivable, the spread is much larger than with α_s.
The relationship between the shallow slab dip and the deformation obliquity, and thus the strain regime, can be interpreted as the expression of the geometrical effect of subduction interface contact on the transmission of forces to the overriding plate and thus on its deformation. A wider plate-to-plate contact, induced by a relatively low value of α_s, promotes compression while the opposite promotes extension. The mean friction coefficient along the subduction interface may modulate this geometrical effect.

IV.1.2. Overriding-plate strain and distance to the slab edge

Schellart (2008a) and Schellart (2024) inferred a direct relationship between the overriding plate deformation rate and the distance to the proximal subducting plate edge from a compilation of geodetic and geologic 1-d (i.e. trench normal) deformation rates at present-day subduction zones. Extension rates were found to be higher close to a slab edge and decrease away from the edge, while compression rates were found to follow the opposite trend. Such observations were explained by analog and numerical models showing that a mantle toroidal flow around slab edges can facilitate the slab rollback near the edges while preventing rollback far from the edges, especially in wide subduction zones (Schellart & Moresi, 2013; Stegman et al., 2006; Sternai et al., 2014).

Taking our 213 subduction transects with a defined non-zero value of v_d, we observe that the highest deformation rates (> 50 mm/yr) generally lie within the first two thousands of kms from a slab edge, regardless of the strain class (Figure 12 a,b). This observation appears to apply to all tectonic regimes, although we note slightly less scatter at low distance for dominant extensive regimes.

Restraining the analysis to major subduction zones, the general trend still holds when taking the transects as a whole (Figure 12 c). However, a more detailed analysis of the trench-normal deformation velocity (v_{d_n}) region per region, gives different insights (Figure 12d). We observe that the decrease in trench-normal extension with increasing distance to the slab edge is clearly observable for the Tonga-Kermadec subduction zone, where the highest extension rates are found in the Lau Basin and decrease southward towards the Havre Trough. This is also the case for the Ryukyus where the spreading rates decrease from west to east. On the contrary, in the Marianas-Izu-Bonin system the trench-normal extension is the highest in Central Marianas and decrease both north- and south-wards. For the Andaman and the Sandwich trenches, there is no obvious trend. Among the settings of dominant compression, the Andes show an increase in trench-normal compression rate with increasing distance to the slab edge, with the highest values observed in the C-Andes (Altiplano region). Likewise trench-normal compression rates are higher in C-Japan and decrease towards the Kurils. On the contrary, high compression rates are observed in Alaska, close to the slab edge, and decrease west-wards towards W- and C-Aleutians, where the regimes switch to dominant strike-slip. Overall, as also discussed by previous studies, our estimation of overriding-plate deformation in systems under dominant compression and extension suggest that the model in which mantle toroidal flow exerts a prime effect on surface deformation may be invoked for only certain subduction zones (Tonga-Kermadec, Ryukyus, the C-Andes), but appear inefficient for explaining the observations in others (e.g. Marianas, Alaska-Aleutians).

One of the novelties of our work is that our kinematic database permits to classify subduction zones under a dominant strike-slip regime, which differs from those in the neutral regime. For the transects under the strike-slip class, only those which correspond to regions of oceanic spreading in directions diverting from the trench normal, exhibit high values of deformation within the first thousands of kms of the slab edge (e.g. Nmost-Tonga, New Hebrides, Smost-Marianas, the Nmost and Smost-Sandwich). Other region in the strike-slip regime, such as Andaman-Sumatra-Java, Central America, or Southern Chile, do not show any trend with the distance to the slab edge. These observations suggest that mantle flow (alone) is difficult to invoke to explain the lateral deformation in subduction zones experiencing strike-slip dominant regime.

IV.1.3. Previous studies on strain partitioning

Early studies suggest that strain partitioning at oblique subduction zones, involving the motion of a forearc sliver, were mainly controlled by the convergence obliquity (e.g. Fitch 1972) and propose the existence of a threshold convergence angle above which such partitioning could occur (Jarrard, 1986; McCaffrey 1992). Following later studies (Turner et al., 2007; Hoffmann-Rothe, et al., 2006; Cooke et al., 2020; Morell et al., 2025), we show that the idea of an obliquity threshold is questionable and that trench-parallel overriding-plate deformation can occur at any value of convergence obliquity (Figure 8). We, however, highlight that there is a certain tendency to increase trench-parallel deformation rate with the increase of the trench-parallel convergence velocity (Figure 9) for areas under dominant strike-slip regime. We also show that the degree of lateral partitioning p_t shows little sensitivity to the convergence obliquity (Figure 10). It is also worth noting that, in contrast to what was suggested by Jarrard (1986), we do not detect any specificity of intra-oceanic versus sub-continental subductions in terms of degree of partitioning of deformation, which might suggest that the rheological profile of the overriding plate is not a critical factor. Finally, as noted above, some geographical coincidence exists (2/3 of the cases) between the region undergoing a strong lateral partitioning of deformation and the subduction of prominent bathymetric features. Overall, our statistical analysis may depict a conceptual model where it is rather the “friction” along the plate interface which plays a key role in defining partitioning, as previously proposed (e.g. Chemenda et al. 2000). In such a conceptual model, the subduction of bathymetric features could enhance the effective long-term “friction” at the interplate contact. It is however beyond the scope of the paper to further assess this hypothesis and will be the focus of later works.

Recently, Morell et al. (2025) have specifically analyzed the arc and forearc active deformation through computation of the vorticity of GNSS velocities, for major subduction zones amounting to a total length of 24 000 km of present-day subduction zones (about half of the total). A main result of their work is that a low to moderate obliquity can lead to strain partitioning (see above). Furthermore, their sampled subduction zones show that the vorticity tends to increase with convergence obliquity. Our sampling of ~45 000 km of subduction zones for which we have a constrained value of overriding-plate deformation, shows a weak relationship between the convergence and the deformation obliquities, and confirms that low obliquities can lead to a wide range of deformation obliquity. In addition, the finding on the relationship between GNSS vorticity and convergence obliquity by Morell et al., (2025) may be compared to our observation that the trench-parallel component of deformation velocity tends to increase with that of the convergence velocity for our 90 transects under a dominant strike-slip regime with values of lateral partition coefficient below of equal to 1 (~19 000 km in terms of length, non-transparent dots on Figure 9). Overall, our study confirms the main conclusions of Morell et al. (2025), showing that they also apply to other subduction zones not considered in their study.

IV.2. Consequences for the revised subduction velocities

Accounting for an overriding plate deformation velocity v_d, we are able to correct the convergence velocities v_c inferred from global plate models, and to assess a better estimate of the rate of SP consumption at trench, that is the subduction velocity $v_s = v_c + v_d$. The values of v_s impact the estimates of mass transfers in present-day subduction zones, including that of volatiles (von Huene & Scholl, 1991; Lallemand et al., 2024), of the thermal structure of the subducting plate via the thermal parameter (Kirby et al., 1996), and of the seismic potential of the subduction megathrust (Scholz & Campos, 1995; Wirth et al., 2022). Moreover, thermo-mechanical models of subduction zones often use the estimations subduction velocities as input parameters, with consequence on the estimations of the thermal structure of present-day subduction zones (e.g. Syracuse et al., 2010), that of the release-depth of volatiles (Cerpa et al., 2022a; Van Keken et al., 2011), or that of the interface strength (Fraters et al., 2025). Other indirect impacts through numerical modeling, would be the assessment of the dynamics of plate-mantle coupling (Arcay, 2012; Turino & Holt, 2024), of the deformation of the overriding plate (Cerpa et al., 2018), and of the slab-dynamics in the mantle transition zone (Cerpa et al., 2022b). For obvious reasons, it is beyond the scope of this contribution, to re-assess or discuss all of these estimates. Here, we thus made the choice to illustrate the changes induced by the account of the overriding plate deformation on the thermal parameter and on the slip length.

IV.2.1. Thermal parameter

The thermal parameter φ is generally used as a first-order estimation of the slab-thermal structure. It has been shown to correlate with the seismogenic potential within the slab especially of intermediate-depth earthquakes (Kirby et al., 1996; Stein & Stein, 1996; Wiens & Gilbert, 1996). Its value, expressed in km, is the product of the slab's rate of descent, $v.\sin\alpha$ in km/m.y., α being the slab's dip, and its age in millions of years. We thus calculate the thermal parameter for transects that have a defined convergence/subduction kinematics, slab age and slab dip (Figures 13a,b). Note that for the slab dip, we use the average of α_s and α_d, and we take the trench-normal components of velocities. We also compute the difference between the thermal parameter calculated using v_{c_n} and that using v_{s_n} (Figures 13c). Different values of the thermal parameters are reached for 155 of our transects (where $v_{d_n} \neq 0$).

The most striking differences between the calculations of the thermal parameter are for the transects undergoing moderate to fast back-arc spreading, such as in Tonga, the Marianas and the Aegean where the thermal parameter increase by a factor of two to three if we use v_{s_n} instead of v_{c_n}. For the Sandwich transects, the difference is up to an order of magnitude. In addition, transects that undergo an important compression deformation rate, such as those in N-New-Hebrides or those where the overriding plate deformation represents a retro-subduction zone (Timor, Philippines), also lead to important deformation rates and thus relatively important decrease in the estimations of the thermal parameter if one uses v_{s_n}. Overall, comparing the two possibilities for estimating the thermal parameter, we find that approximately in 70% of the cases the change in thermal parameter are of absolute values of 10^3 km or less. In 10% of cases the absolute difference is between 10^3 and 2×10^3 km, , among which ~70% and ~35% are under dominant extension and strike-slip, respectively. In 10% of cases between 2×10^3 and 3×10^3, among which ~70% and ~20% are under dominant extension and strike-slip, respectively. In the remaining 10% of cases the absolute difference is between 3×10^3 km and up to 9×10^3 km, with 80% and 20% of transects being under dominant extension and strike-slip, respectively. The latter cases are mostly transects undergoing fast back-arc spreading.

IV.2.2. Slip length

For a given seismogenic zone width, the slip length on the megathrust is ideally determined by the angle at which the subducting plate actually enters the trench, that is O_{vs}. When $O_{vc} \simeq O_{vs}$ estimating the slip length using global plate circuit models is a reasonable approach. However, in the case of important strain-partitioning and, for instance, activation of slip on a strike-slip fault, a reduction in the slip length on the seismogenic interface is expected.

Using our up-to-date kinematic database, we can compare the estimations of slip length using the convergence L_{vc} and that using the subduction velocity L_{vs}. Figure 14 shows areas where the reduction in slip length due to arc blocks deformation exceeds 10%, and reaches in extreme cases (New Britain, Andaman) as much as 80-90%. These sectors represent 16.5% of subduction zone transects, two-third of which were not covered by MORVEL56 (underlined transects in Figure 14). As an example, the Smost section of the Ryukyu subduction zone deforms in a way that the slip length across the seismogenic zone is decreased by more than 60%. This reduction reaches 20% in the Nankai trough, 35% in W-Aleutians, 10 to 30% in Central-Aleutians or 10 to 15% in Sumatra.

V. Conclusion and perspective

We have built a new database of overriding-plate deformation in present-day subduction zones, consistently based on geodetic data. Our kinematic description of overriding-plate deformation, through the motion of an “arc block” relative to an undeformed upper plate, permits to characterize both the trench-normal and the trench-parallel components of deformation. Our analysis confirms that the obliquity of convergence generally leads to a lateral (quasi-trench parallel) deformation in the overriding plate, which we interpret as the evidence of a lateral shear component on the subduction interface. However, we demonstrate that there is not a straightforward relationship between the convergence obliquity and the degree of (lateral) strain partitioning. Other subduction characteristics, such as the subduction of large oceanic reliefs may largely contribute to shear on the interface and thus trigger lateral deformation in the overriding plate. Furthermore, although there are a few counter-examples, we also confirm the trend that the dip of a slab, especially for depths lesser than 125 km, correlates with the deformation regime of the overriding plate (low values of slab dip leading to compression, high values to extension, and intermediate to strike-slip).

Finally, our estimations of overriding plate deformation permit an enhancement of the estimation of subducting-plate consumption rates at the trenches, relative to studies using instead estimations based on far-field (convergence) relative velocities. This has implications for the predictions of mass transfers from the surface to the mantle, the thermal structure of the slab, the shear on the subduction interface, or seismic coupling, insofar as the slip along the subduction interface predicted by kinematics is compared with seismic slip.

Acknowledgements

This research received funding from the programme TelluS of the Institut National des Sciences de l'Univers, CNRS, awarded to N. Cerpa.

Author contributions

Conceptualization - N. Cerpa, S. Lallemand

Methodology – N. Cerpa, S. Lallemand

Investigation – N. Cerpa

Data Curation - N. Cerpa, S. Lallemand

Formal Analysis – N. Cerpa

Original draft – N. Cerpa

Review & Editing - N. Cerpa, S. Lallemand, A. Heuret

Visualization – N. Cerpa, S. Lallemand

Data availability

Our database will be made available through our webtool submap (www.submap.fr).

Conflict interests

The authors declare no competing interests.

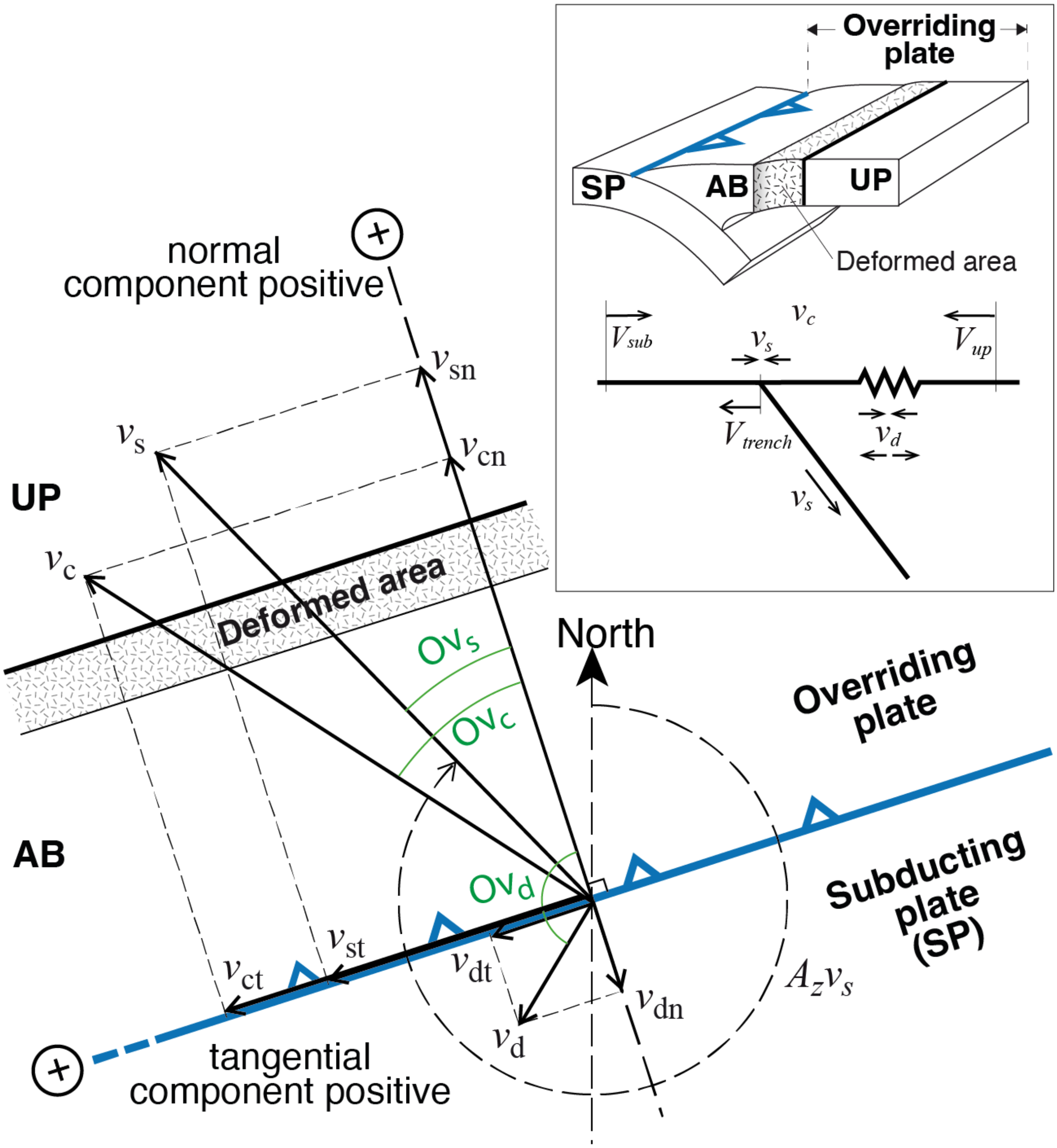

Figure 1: Conventions used in the geometrical and kinematical description of the subduction transects in the Submap database. UP = upper plate, AB = arc block, SP = subducting plate, v_c: convergence velocity, v_s: subduction velocity, v_d: deformation velocity. The indices $_n$ and $_t$ denote the normal and tangential components, respectively, of the vectors. O_{vx} stands for the obliquity and $A_z v_x$ for azimuth of the velocities.

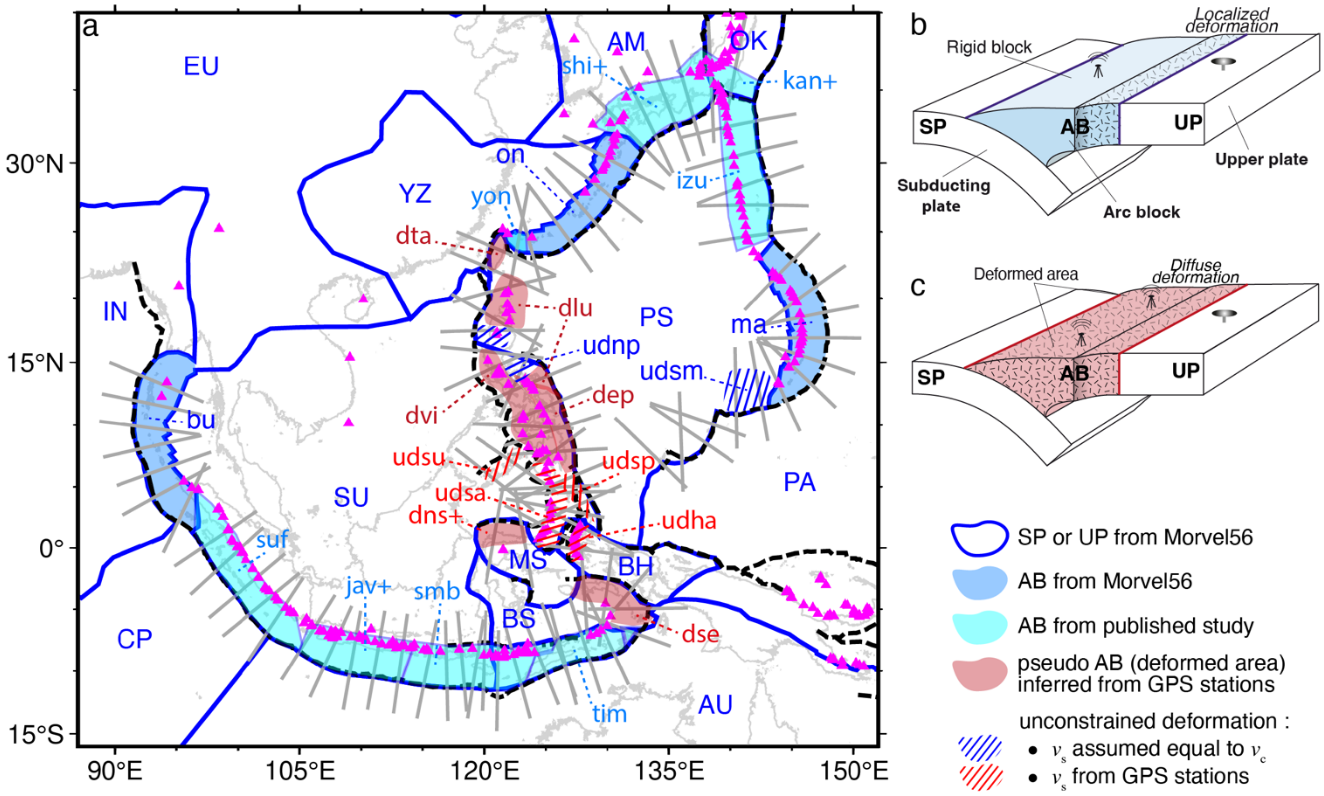

Figure 2: Major plates and arc blocks in the Southeast-Asia region (a) and schematic illustration of two ways of assessing the AB motion (b,c). Thick blue lines represent the contours of the major plates from MORVEL56 which are used to define our SP and UP. Dark-blue filled regions represent the AB from MORVEL56. Light-blue filled regions represent the AB that we introduce from published studies. Red-patches represent the regions where we found single GPS velocities (no-block motion defined) and which we have used to either estimate v_d (pseudo-rigid blocks). In few cases, v_c is undefined but v_s can be estimated from GPS stations (red stripes). The abbreviations of plates and block names are listed in Table 1. Blue-stripe areas indicate regions where geological-evidence of deformation exists but where we have not found geodetic data to characterize the deformation. We thus assume $v_s = v_c$. The gray straight lines represent the subduction transects used in our study (i.e. the submap transects). Black dashed lines are the subduction trenches

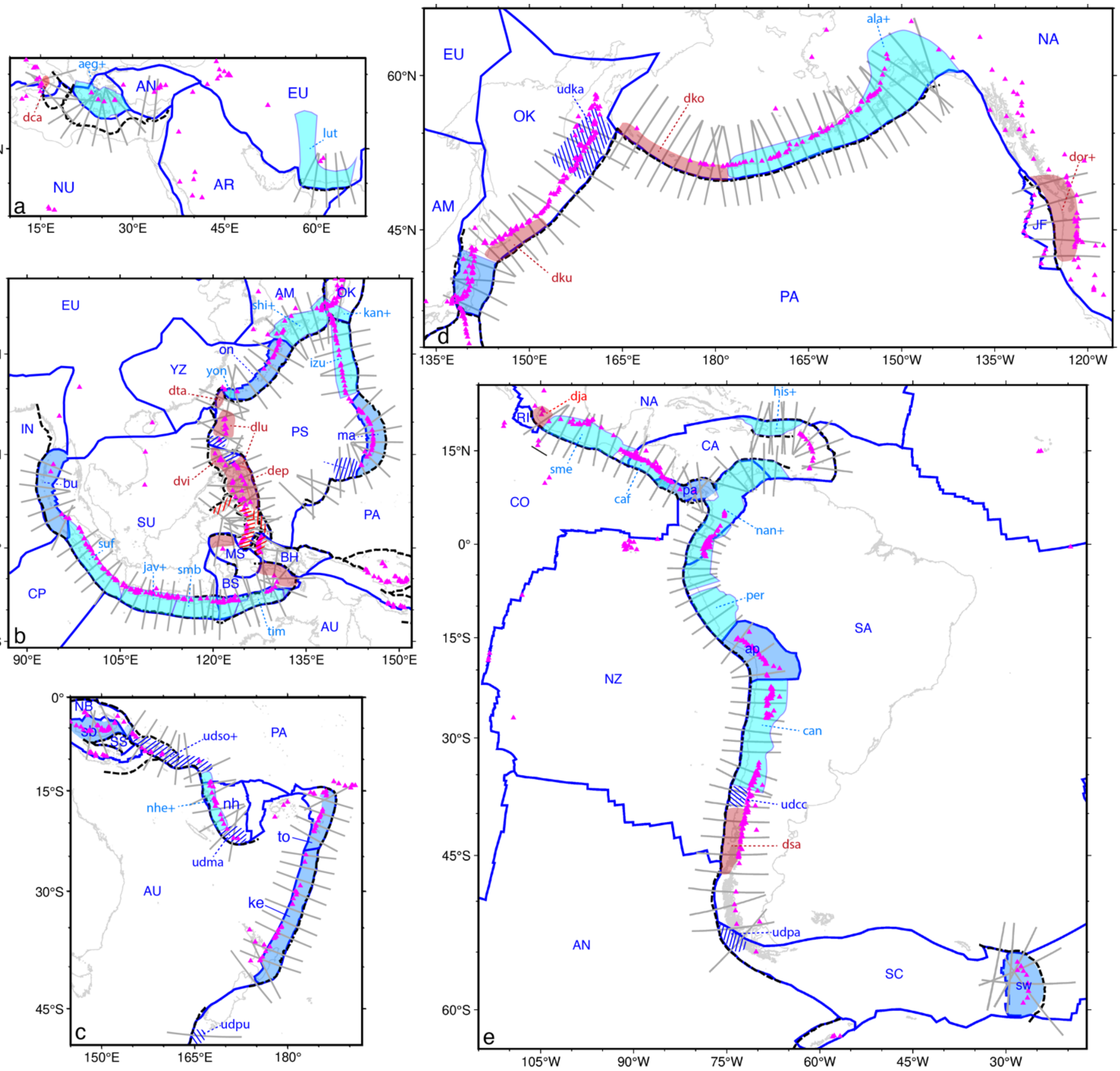

Figure 3 Maps with all AB and deformed regions accounted for in our kinematic database (a- Mediterranean and Makran, b- Southeast Asia, c- Southwest Pacific, d- North Pacific, e- Central & South America, Caribbeans & South-Sandwich.). See Figure 2 for legend details.

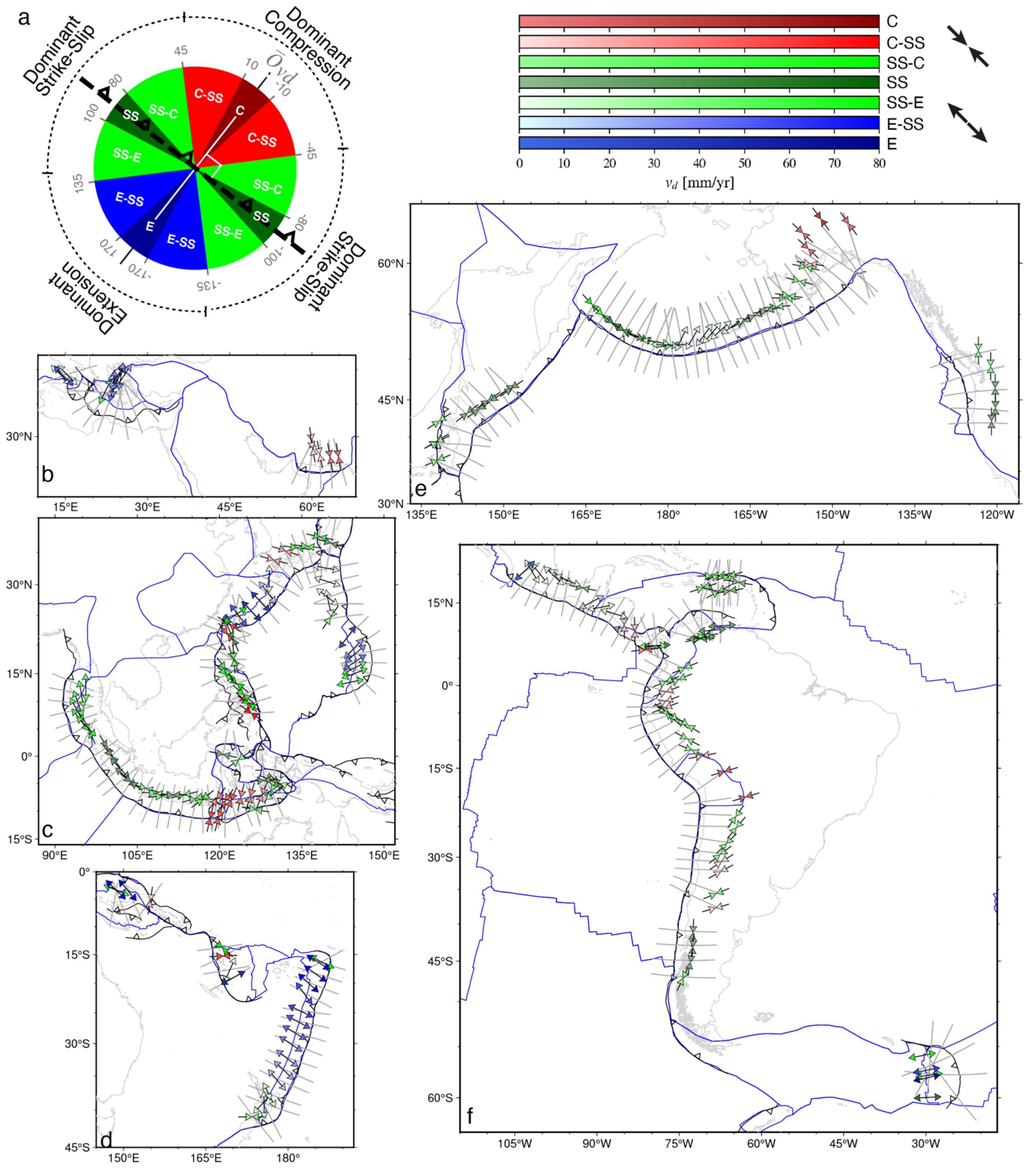

Figure 4. Maps of the deformation velocity vector v_d represented at the intersection between the subducction transects and the inner boundaries of the arc blocks, and colored by the magnitude and the associated strain regime. The top-left diagram illustrates the classes of strain (dominant) regimes defined as a function of the directed obliquity $\bar{O}_{v_d}$ between the trench-normal and v_d.

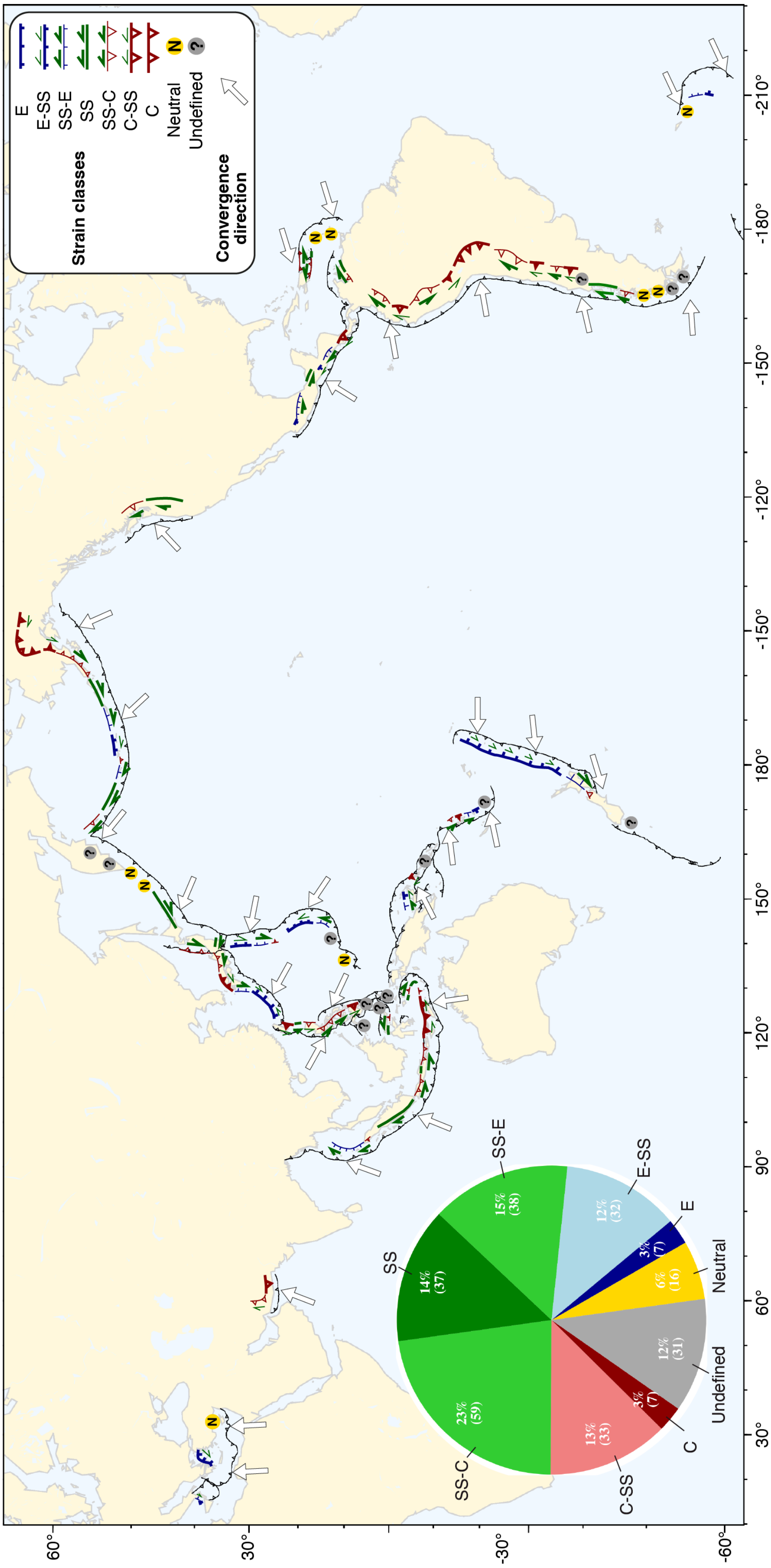
Strain classes
E
E-SS
SS-E
SS
SS-C
C-SS
C
Neutral
Undefined
Convergence direction
SS-E
15% (38)
E-SS
12% (32)
E
3% (7)
Neutral
6% (16)
Undefined
12% (31)
C
3% (7)
C-SS
13% (33)
SS-C
23% (59)
SS
14% (37)

Figure 5. Schematic global view of the strain classes determined in our study with their distribution (piechart). The symbolic representation of overriding-plate deformation is positioned at the boundary between AB and UP. Note that our representation is intentionally schematic and is not intended to always represent actual geological structures. The azimuth of some faults may therefore not correspond to that obserserved on the field.

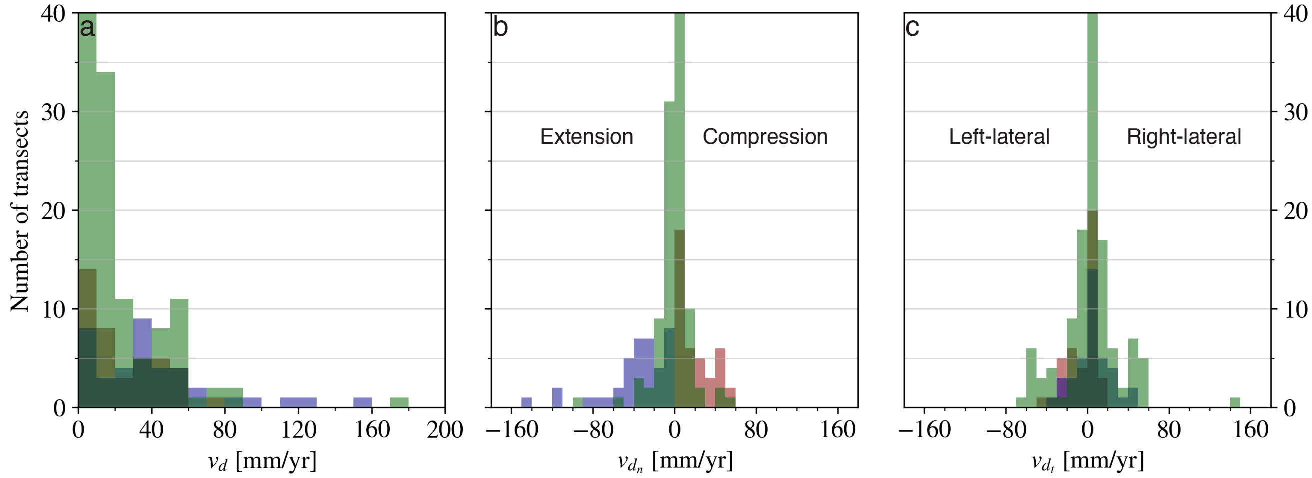

Figure 6. Distribution of overriding plate deformation rates determined for all transect of the Submap database. a) magnitude of deformation velocity v_d, b) normal component $v_{d_n}$of deformation velocity, tangential component v_{d_t} of the deformation velocity

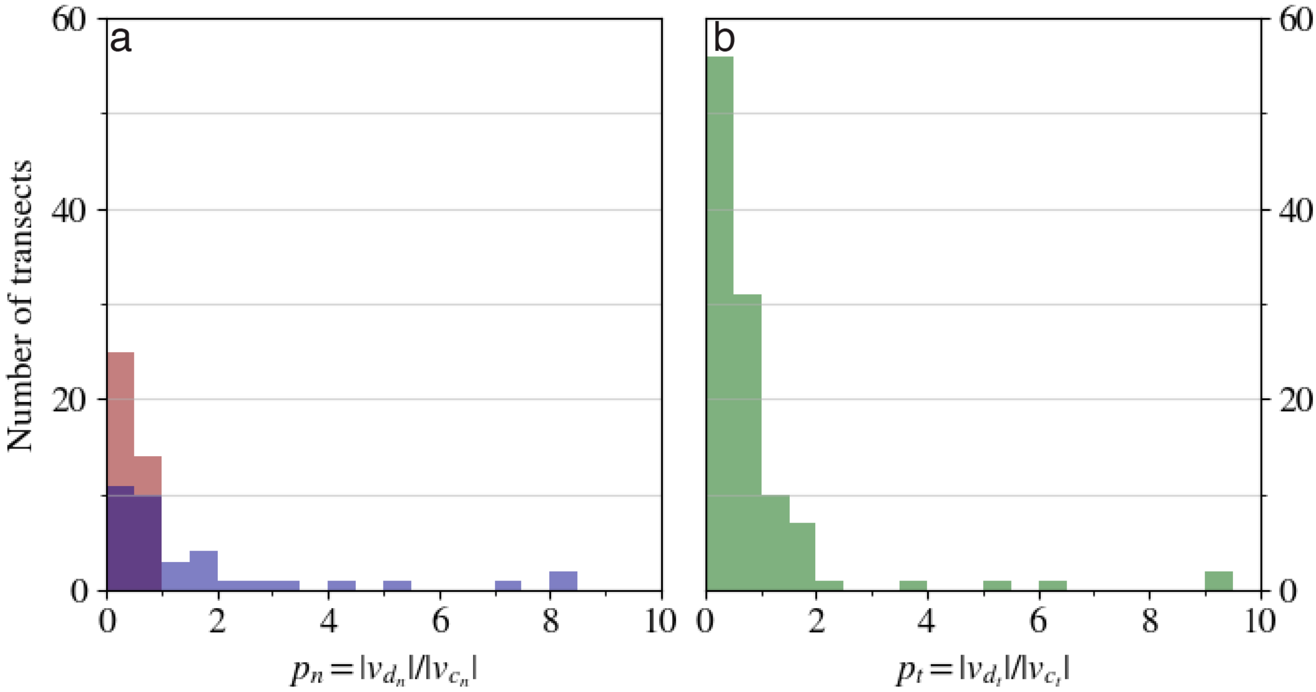

Figure 7. Ratios of the components of overriding plate deformation velocities to the components of the convergence velocities. Other legend details are as in Figure 6.

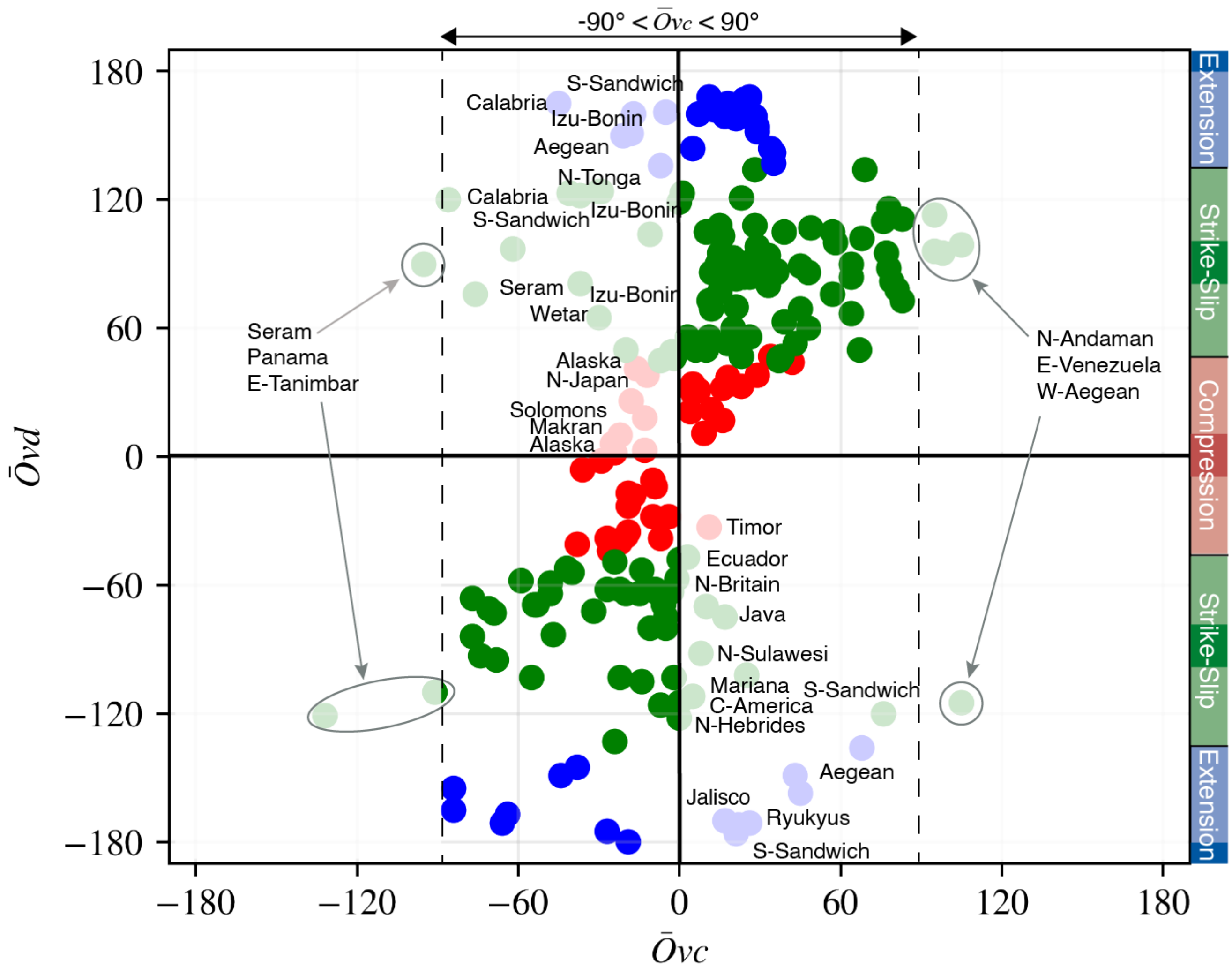

Figure 8. Obliquity of the convergence between major subducting (SP) and upper (UP) plates against the obliquity of deformation for 213 transects with non-null vd. The transects are colored following their Ovd-based tectonic regimes (blue for extension, green for strike-slip and red for compression). The shaded quadrants highlight cases of opposite signs of obliquities, i.e., the transects for which the convergence obliquity fails to explain the deformation obliquity. The regions for which $|O_{vc}| > 90°$ (dotted black line) are also shaded.

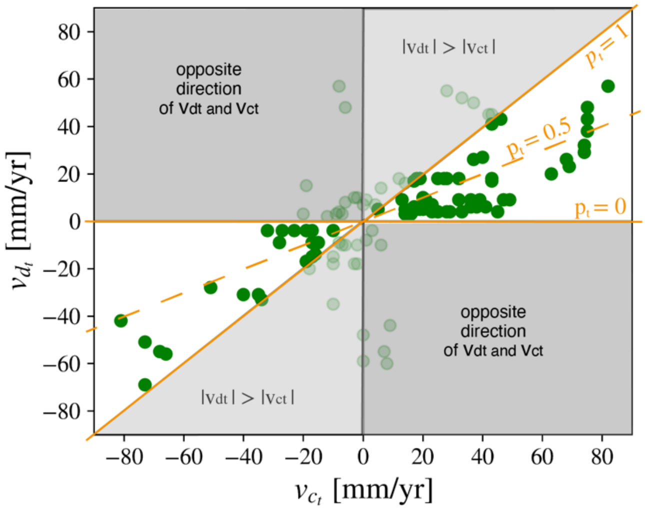

Figure 9. Tangential component of the deformation velocity as a function of the tangential component of the convergence velocity for all transects in the dominant strike-slip regime. The non-transparent green dots are those for which the magnitude of deformation velocity is higher than 1 mm/yr, which have a lateral partition coefficient equal or less than 1, and which have consistent directions of the tangential components of both velocities. Semi-transparent green dots denote all the remaining transects under the dominant strike-slip strain regime.

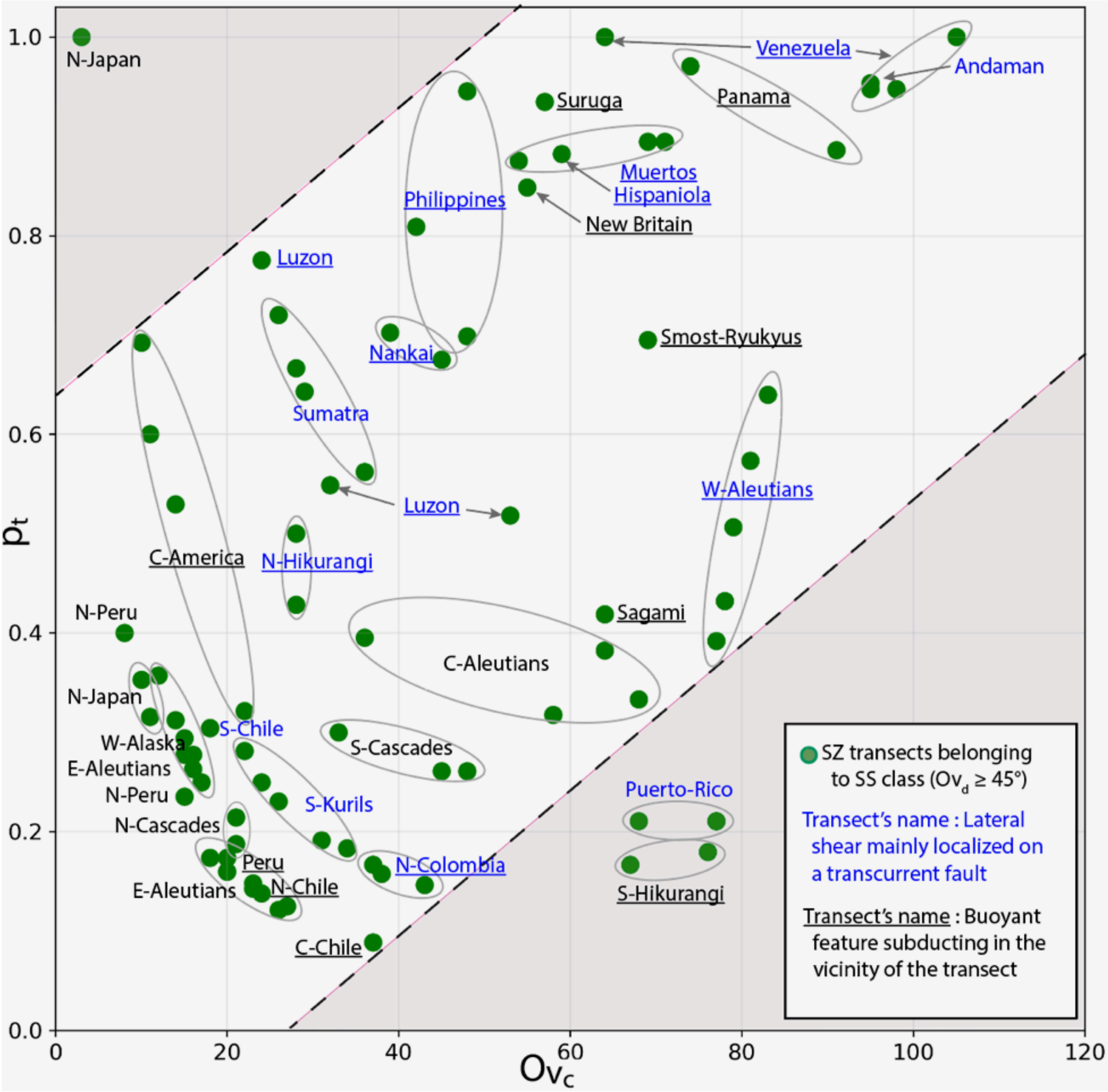

Figure 10. Lateral partition coefficient p_t as a function of convergence obliquity Ov_c for subduction transects under a dominant strike-slip strain class.

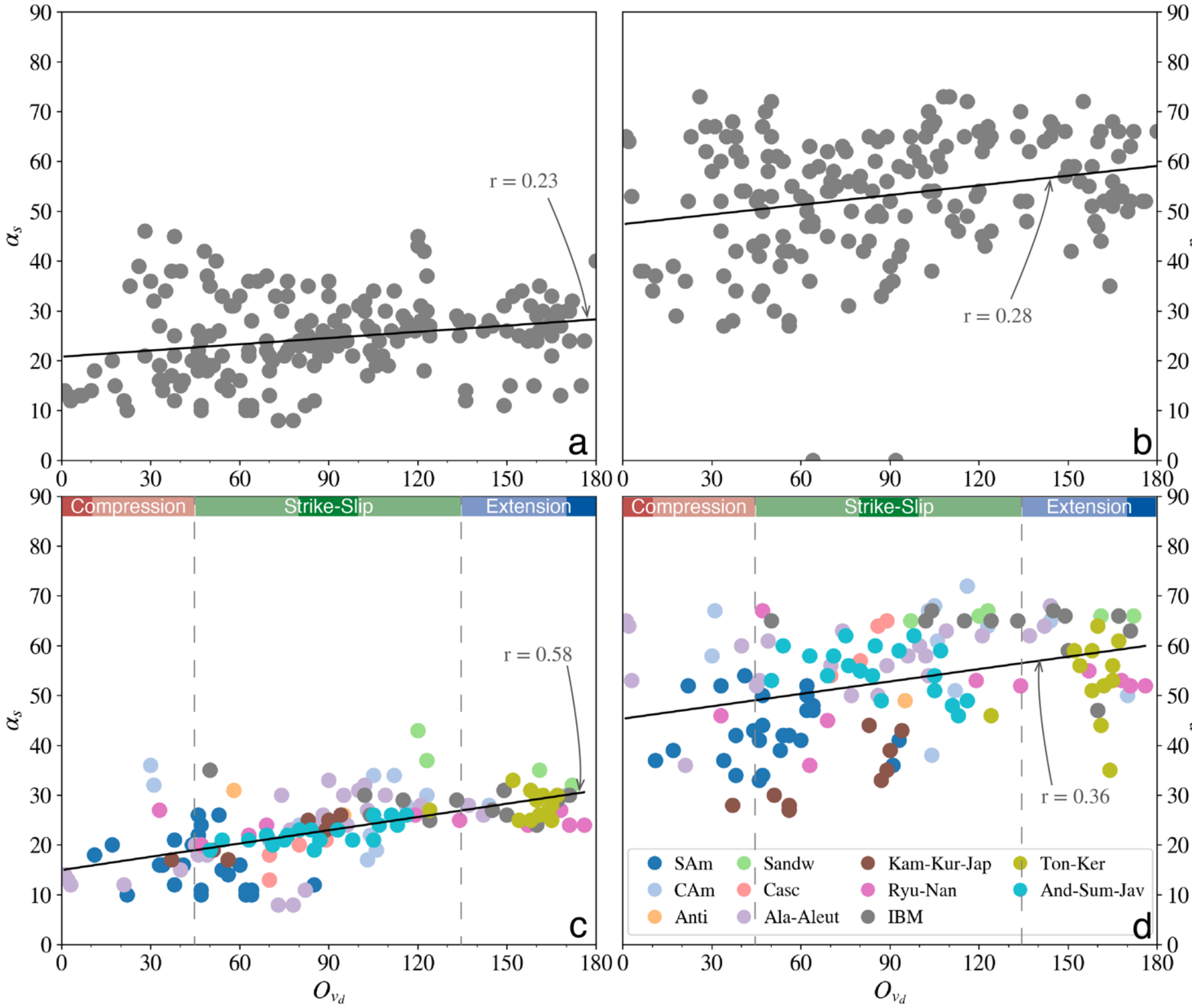

Figure 11. Obliquity of the deformation velocity with shallow (0 to 125 km depth ; left) and deep (125 to 400 km ; right) slap dip for all (top) and selected major (bottom) subduction zones. Sam:South America, CAm:Central America, Anti:Lesser Antilles, Sandw:Sandiwch, Casc: Cascadia, Ala-Aleut:Alaska-Aleutians, Kam-Kur-Jap:Kamchatcka-Kurils-Japan, Ryu-Nan:Ryukyus-Nankai, IBM:Izu-Bonin-Marianas, Ton-Ker:Tonga-Kermadec, And-Sum-Jav:Andaman-Sumatra-Java.

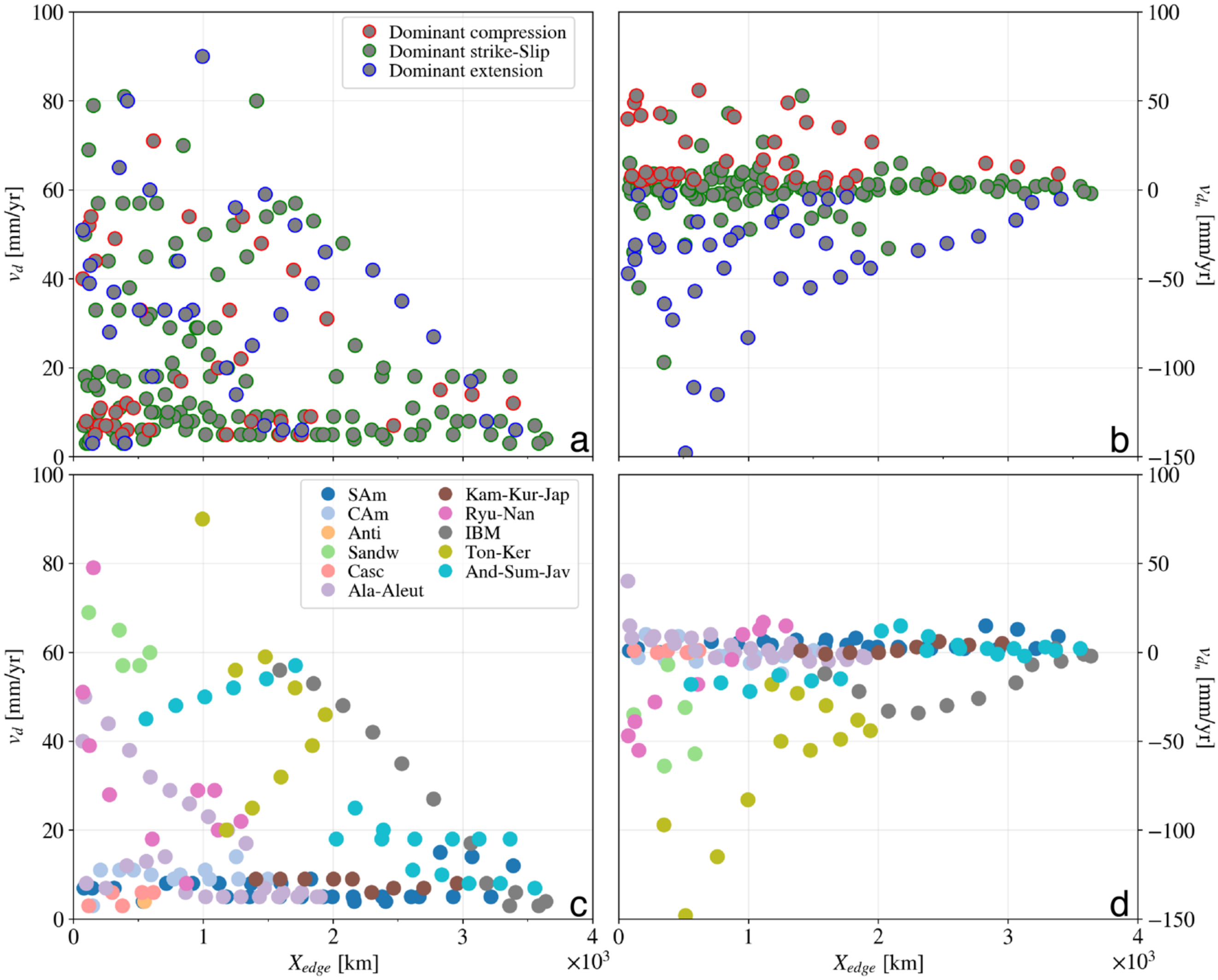

Figure 12. Overriding-plate deformation velocity with distance to the edge of the trench. Left column (a,c) is for total velocity and right column (b,d) for only the trench-normal component. Top rows (a,b) display the values for all 213 subduction transects with definite non-zero values of v_d and the bottom row (c,d) that of 141 transects corresponding to selected subduction zones.

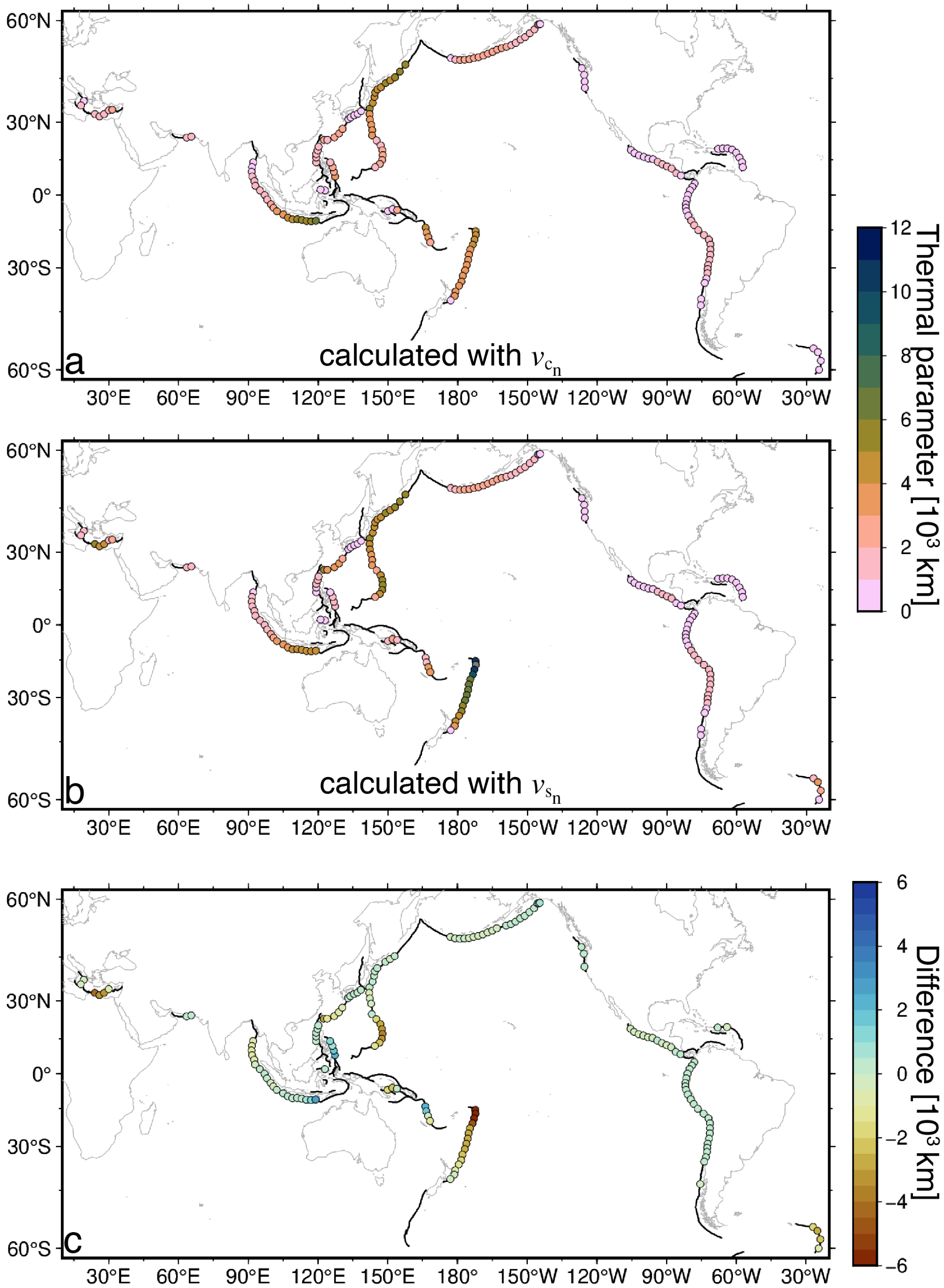

Figure 13. Global map of the thermal parameter calculated using v_c (a) and our revised v_s (b), as well as their difference (c).

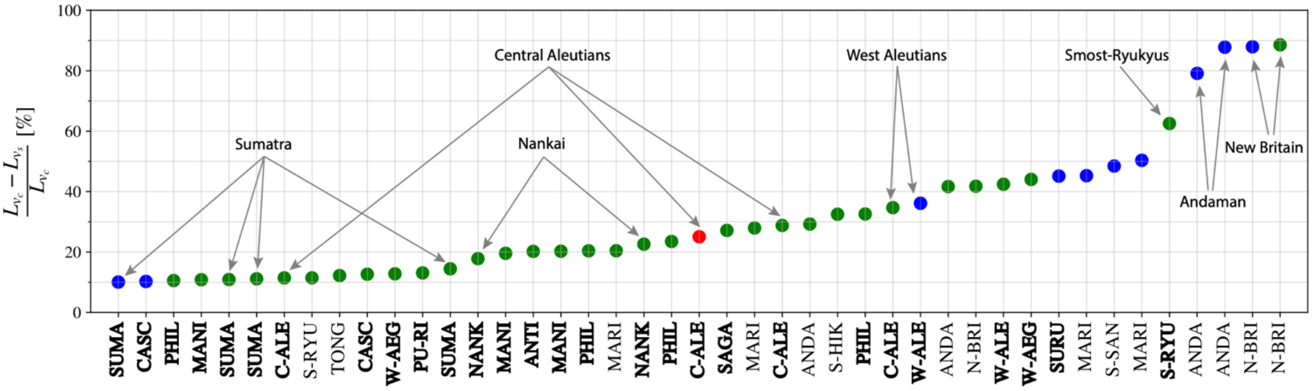

Figure 14. Slip length reduction expected along the subduction (seismogenic) interface using our estimated values of v_s. Transect-names in bold correspond to the transects for which we have added constraints on overriding-plate deformation beyond the MORVEL56 model.

AB types (constrained vd)	Short names incl. aggregates (+)	AB names	Sources	Number of ABs
M56 blocks	ok	OKHOTSK	Argus et al. (2011)	11
	pa	PANAMA	Argus et al. (2011)	
	ap	ALTIPLANO	Argus et al. (2011)	
	sw	SANDWICH	Argus et al. (2011)	
	bu	BURMA	Argus et al. (2011)	
	on	OKINAWA	Argus et al. (2011)	
	ma	MARIANA	Argus et al. (2011)	
	sb	SOUTH BISMARCK	Argus et al. (2011)	
	nb	NORTH BISMARCK	Argus et al. (2011)	
	to	TONGA	Argus et al. (2011)	
	ke	KERMADEC	Argus et al. (2011)	
additional rigid blocks (our compilation)	aeg+	WESTERN PELOPONNESE	Vernant et al. (2014)	35
		AEGEAN SEA	Vernant et al. (2014)	
		RHODES	Vernant et al. (2014)	
		ISPARTA	Vernant et al. (2014)	
	lut	LUT	Reilinger et al. (2006)	
	ala+	PENINSULA	Elliot and Freymueller (2020)	
		KODIAK	Elliot and Freymueller (2020)	
		PRINCE WILLIAM SOUND	Elliot and Freymueller (2020)	
		ICY BAY	Elliot and Freymueller (2020)	
	sme	SOUTHERN MEXICO	Andreani et al., (2008)	
	caf	CENTRAL AMERICAN FOREARC	Carvajal-Soto et al., (2020)	
	nan+	BONAIRE	Jarrin et al. (2023)	
		SAN JACINTO	Jarrin et al. (2023)	
		ROMERAL	Jarrin et al. (2023)	
		NORTH ANDEAN WEST	Jarrin et al. (2023)	
		PERUVIAN FOREARC WEST	Jarrin et al. (2023)	
	his+	HISPANIOLA	Calais et al. (2023)	
		PUERTO-RICO	Calais et al. (2023)	
		NORTH HISPANIOLA	Calais et al. (2023)	
	per	PERU	Villegas-Lanza et al. (2016)	
	can	CENTRAL_ANDES	Brooks et al. (2003)	
	suf	SUMATRA FOREARC	Bradley et al. (2017)	
	jav+	WEST JAVA	Koulali et al. (2017)	
		EAST JAVA	Koulali et al. (2016)	
	smb	SUMBA	Koulali et al. (2016)	
	tim	TIMOR	Koulali et al. (2016)	
	yon	YONAGUNI	Chen et al. (2022)	
	shi+	SHIKOKU	Nishimura et al. (2018)	
		CHUBU	Nishimura et al. (2018)	
	kan+	IZU	Nishimura (2011)	
		KANTO	Nishimura (2011)	
	izu	IZU BONIN ARC	Nishimura (2011)	
	nhe+	NORTH NEW-HEBRIDES	Bergeot et al. (2009)	
		CENTRAL NEW-HEBRIDES	Bergeot et al. (2009)	
		SOUTH NEW-HEBRIDES	Bergeot et al. (2009)	
additional deformed areas (vd based on GPS stations, our compilation)	dca	DEF_CALABRIAN ARC	Serpelloni et al. (2009)	14
	dku	DEF_KURIL FOREARC	Demets (1992)	
	dko	DEF_KOMANDORSKY FOREARC	Cross and Freymueller (2008)	
	dor+	DEF_VANCOUVER ISLAND	Mazzotti et al. (2003)	
		DEF_OREGON	Mazzotti et al. (2002)	
	dja	DEF_JALISCO	Selvans et al. (2010)	
	dsa	DEF_SOUTH ANDES	Wang et al., (2007)	
	des	DEF_SERAM	Rangin et al. (1999)	
	dns+	DEF_MANADO	Socquet et al. (2006)	
		DEF_NORTH SULA	Socquet et al. (2006)	
	dep	DEF_EAST PHILIPPINES	Rangin et al. (1999)	
	dlu	DEF_LUZON	Hsu YJ (pers. comm. 2023)	
	dvi	DEF_VISAYAS	Simons et al. (2007)	
	dta	DEF_TAIWAN	Hsu YJ (pers. comm. 2023)	
Total				**60**

Table 1: List of "arc blocks", including the short names as they appear in Figures 2 and 3. The symbol "+" stands for cases where we have merged together several blocks into a single one on the figures.

AB types (unconstrained vd)	Short names incl. aggregates (+)	AB names	Sources	number of ABs
deformed areas with GPS-derived vs and undefined vc (our compilation)	udha udsa udsp udsu	UNDEF_HALMAHERA ARC UNDEF_SANGIHE ARC UNDEF_SOUTH PHILIPPINES UNDEF_SULU ARC	Rangin et al. (1999) Rangin et al. (1999) Rangin et al. (1999) Simons et al. (2007)	**4**
deformed areas with M56-derived vc and used as a proxy for vs, assuming vd to be small (our compilation)	udka udcc udpa udsm udnp udso+ udma udpu	UNDEF_KAMCHATKA UNDEF_CENTRAL CHILE UNDEF_SOUTH PATAGONIA UNDEF_SOUTH MARIANA UNDEF_NORTH PHILIPPINES UNDEF_SOLOMONS UNDEF_SANTA-CRUZ UNDEF_MATTHEW ISLAND UNDEF_PUYSEGUR		**9**
Total				**13**

Table 2 : List of complementary areas where we have derived subduction velocities without any constraints on the deformation velocity.

References

Alvarado, A., Audin, L., Nocquet, J. M., Jaillard, E., Mothes, P., Jarrín, P., et al. (2016). Partitioning of oblique convergence in the Northern Andes subduction zone: Migration history and the present-day boundary of the North Andean Sliver in Ecuador. *Tectonics*, *35*(5), 1048–1065. https://doi.org/10.1002/2016TC004117

Andreani, L., Le Pichon, X., Rangin, C., & Martínez-Reyes, J. (2008). The southern Mexico block: main boundaries and new estimation for its Quaternary motion. *Bulletin de La Société Géologique de France*, *179*(2), 209–223. https://doi.org/10.2113/gssgfbull.179.2.209

Arcay, D. (2012). Dynamics of interplate domain in subduction zones: influence of rheological parameters and subducting plate age. *Solid Earth*, *3*(2), 467–488. https://doi.org/10.5194/se-3-467-2012

Argus, D. F., Gordon, R. G., & DeMets, C. (2011). Geologically current motion of 56 plates relative to the no-net-rotation reference frame: NNR-MORVEL56. *Geochemistry, Geophysics, Geosystems*, *12*(11), n/a-n/a. https://doi.org/10.1029/2011GC003751

Baize, S., Audin, L., Alvarado, A., Jomard, H., Bablon, M., Champenois, J., et al. (2020). Active Tectonics and Earthquake Geology Along the Pallatanga Fault, Central Andes of Ecuador. *Frontiers in Earth Science*, *8*. https://doi.org/10.3389/feart.2020.00193

Barrier, E., Huchon, P., & Aurelio, M. (1991). Philippine fault: A key for Philippine kinematics. *Geology*, *19*(1), 32–35. https://doi.org/10.1130/0091-7613(1991)019<0032:PFAKFP>2.3.CO;2

Becker, T. W., Schaeffer, A. J., Lebedev, S., & Conrad, C. P. (2015). Toward a generalized plate motion reference frame. *Geophysical Research Letters*, *42*(9), 3188–3196. https://doi.org/10.1002/2015GL063695

Bellier, O., & Sébrier, M. (1995). Is the slip rate variation on the Great Sumatran Fault accommodated by fore-arc stretching? *Geophysical Research Letters*, *22*(15), 1969–1972. https://doi.org/10.1029/95GL01793

Bergeot, N., Bouin, M. N., Diament, M., Pelletier, B., Régnier, M., Calmant, S., & Ballu, V. (2009). Horizontal and vertical interseismic velocity fields in the Vanuatu subduction zone from GPS measurements: Evidence for a central Vanuatu locked zone. *Journal of Geophysical Research: Solid Earth*, *114*(B6), 2007JB005249. https://doi.org/10.1029/2007JB005249

Bradley, K. E., Feng, L., Hill, E. M., Natawidjaja, D. H., & Sieh, K. (2017). Implications of the diffuse deformation of the Indian Ocean lithosphere for slip partitioning of oblique plate convergence in Sumatra. *Journal of Geophysical Research: Solid Earth*, *122*(1), 572–591. https://doi.org/10.1002/2016JB013549

Brizzi, S., Sandri, L., Funiciello, F., Corbi, F., Piromallo, C., & Heuret, A. (2018). Multivariate statistical analysis to investigate the subduction zone parameters favoring the occurrence of giant megathrust earthquakes. *Tectonophysics*, *728–729*, 92–103. https://doi.org/10.1016/j.tecto.2018.01.027

Brooks, B. A., Bevis, M., Smalley, R., Kendrick, E., Manceda, R., Lauría, E., et al. (2003). Crustal motion in the Southern Andes (26°–36°S): Do the Andes behave like a microplate? *Geochemistry, Geophysics, Geosystems*, *4*(10), 2003GC000505. https://doi.org/10.1029/2003GC000505

Byrne, D. B., Suarez, G., & McCann, W. R. (1985). Muertos Trough subduction—microplate tectonics in the northern Caribbean? *Nature*, *317*(6036), 420–421. https://doi.org/10.1038/317420a0

Calais, E., Symithe, S. J., & de Lépinay, B. M. (2022). Strain Partitioning within the Caribbean–North America Transform Plate Boundary in Southern Haiti, Tectonic and Hazard Implications. *Bulletin of the Seismological Society of America*, *113*(1), 131–142. https://doi.org/10.1785/0120220121

Carvajal-Soto, L. A., Ito, T., Protti, M., & Kimura, H. (2020). Earthquake potential in Costa Rica using three scenarios for the central Costa Rica deformed belt as western boundary of the Panama microplate. *Journal of South American Earth Sciences*, *97*, 102375. https://doi.org/10.1016/j.jsames.2019.102375

Cerpa, N. G., Guillaume, B., & Martinod, J. (2018). The interplay between overriding plate kinematics, slab dip and tectonics. *Geophysical Journal International*, *215*(3), 1789–1802. https://doi.org/10.1093/gji/ggy365

Cerpa, N. G., Arcay, D., & Padrón-Navarta, J. A. (2022a). Sea-level stability over geological time owing to limited deep subduction of hydrated mantle. *Nature Geoscience*, *15*(5), 423–428. https://doi.org/10.1038/s41561-022-00924-3

Cerpa, N. G., Sigloch, K., Garel, F., Heuret, A., Davies, D. R., & Mihalynuk, M. G. (2022b). The Effect of a Weak Asthenospheric Layer on Surface Kinematics, Subduction Dynamics and Slab Morphology in the Lower Mantle. *Journal of Geophysical Research: Solid Earth*, *127*(8), e2022JB024494. https://doi.org/10.1029/2022JB024494

Chemenda, A., Lallemand, S., & Bokun, A. (2000). Strain partitioning and interplate friction in oblique subduction zones: Constraints provided by experimental modeling. *Journal of Geophysical Research: Solid Earth*, *105*(B3), 5567–5581. https://doi.org/10.1029/1999JB900332

Chen, H.-Y., Hsu, Y.-J., Ikuta, R., Tung, H., Tang, C.-H., Ku, C.-S., et al. (2022). Strain Partitioning in the Southern Ryukyu Margin Revealed by Seafloor Geodetic and Seismological Observations. *Geophysical Research Letters*, *49*(6), e2022GL098218. https://doi.org/10.1029/2022GL098218

Collot, J.-Y., Lamarche, G., Wood, R. A., Delteil, J., Sosson, M., Lebrun, J.-F., & Coffin, M. F. (1995). Morphostructure of an incipient subduction zone along a transform plate boundary: Puysegur Ridge and Trench. *Geology*, *23*(6), 519–522. https://doi.org/10.1130/0091-7613(1995)023<0519:MOAISZ>2.3.CO;2

Cooke, M. L., Toeneboehn, K., & Hatch, J. L. (2020). Onset of slip partitioning under oblique convergence within scaled physical experiments. *Geosphere*, *16*(3), 875–889. https://doi.org/10.1130/GES02179.1

Cross, R. S., & Freymueller, J. T. (2008). Evidence for and implications of a Bering plate based on geodetic measurements from the Aleutians and western Alaska. *Journal of Geophysical Research: Solid Earth*, *113*(B7), 2007JB005136. https://doi.org/10.1029/2007JB005136

DeMets, C. (1992). Oblique convergence and deformation along the Kuril and Japan Trenches. *Journal of Geophysical Research: Solid Earth*, *97*(B12), 17615–17625. https://doi.org/10.1029/92JB01306

Doglioni, C., Carminati, E., Cuffaro, M., & Scrocca, D. (2007). Subduction kinematics and dynamic constraints. *Earth-Science Reviews*, *83*(3–4), 125–175. https://doi.org/10.1016/j.earscirev.2007.04.001

Dominguez, S., Lallemand, S., Malavieille, J., & Schnürle, P. (1998). Oblique subduction of the Gagua Ridge beneath the Ryukyu accretionary wedge system: Insights from marine observations and sandbox experiments. *Marine Geophysical Researches*, *20*(5), 383–402. https://doi.org/10.1023/A:1004614506345

Doubrovine, P. V., Steinberger, B., & Torsvik, T. H. (2012). Absolute plate motions in a reference frame defined by moving hot spots in the Pacific, Atlantic, and Indian oceans. *Journal of Geophysical Research: Solid Earth*, *117*(B9), 2011JB009072. https://doi.org/10.1029/2011JB009072

Elliott, J., & Freymueller, J. T. (2020). A Block Model of Present-Day Kinematics of Alaska and Western Canada. *Journal of Geophysical Research: Solid Earth*, *125*(7), e2019JB018378. https://doi.org/10.1029/2019JB018378

Faccenna, C., Heuret, A., Funiciello, F., Lallemand, S., & Becker, T. W. (2007). Predicting trench and plate motion from the dynamics of a strong slab. *Earth and Planetary Science Letters*, *257*(1–2), 29–36. https://doi.org/10.1016/j.epsl.2007.02.016

Fitch, T. J. (1972). Plate convergence, transcurrent faults, and internal deformation adjacent to Southeast Asia and the western Pacific. *Journal of Geophysical Research (1896-1977)*, *77*(23), 4432–4460. https://doi.org/10.1029/JB077i023p04432

Fraters, M., Billen, M., Naliboff, J., Staisch, L., Watt, J., & Li, H. (2025). Using Subducting Plate Motion to Constrain Cascadia Slab Geometry and Interface Strength. *Geochemistry, Geophysics, Geosystems*, *26*(5), e2024GC011895. https://doi.org/10.1029/2024GC011895

Funiciello, F., Faccenna, C., Heuret, A., Lallemand, S., Di Giuseppe, E., & Becker, T. W. (2008). Trench migration, net rotation and slab–mantle coupling. *Earth and Planetary Science Letters*, *271*(1–4), 233–240. https://doi.org/10.1016/j.epsl.2008.04.006

Gardner, T. W., Fisher, D. M., Morell, K. D., & Cupper, M. L. (2013). Upper-plate deformation in response to flat slab subduction inboard of the aseismic Cocos Ridge, Osa Peninsula, Costa Rica. *Lithosphere*, *5*(3), 247–264. https://doi.org/10.1130/L251.1

Gutscher & Lallemand. (1999). Birth of a major strike-slip fault in SW Japan. *Terra Nova*, *11*(5), 203–209. https://doi.org/10.1046/j.1365-3121.1999.00247.x

Haq, S. S. B., & Davis, D. M. (2010). Mechanics of fore-arc slivers: Insights from simple analog models. *Tectonics*, *29*(5). https://doi.org/10.1029/2009TC002583

Hayes, G. P., Moore, G. L., Portner, D. E., Hearne, M., Flamme, H., Furtney, M., & Smoczyk, G. M. (2018). Slab2, a comprehensive subduction zone geometry model. *Science*, *362*(6410), 58–61. https://doi.org/10.1126/science.aat4723

Heuret, A. (2005, November 16). *Dynamique des zones de subduction : étude statistique globale et approche analogique.* (phdthesis). Université Montpellier II - Sciences et Techniques du Languedoc. Retrieved from https://theses.hal.science/tel-00108728

Heuret, A., & Lallemand, S. (2005). Plate motions, slab dynamics and back-arc deformation. *Physics of the Earth and Planetary Interiors*, *149*(1–2), 31–51. https://doi.org/10.1016/j.pepi.2004.08.022

Heuret, A., Lallemand, S., Funiciello, F., Piromallo, C., & Faccenna, C. (2011). Physical characteristics of subduction interface type seismogenic zones revisited: SUBDUCTION-TYPE SEISMOGENIC ZONES. *Geochemistry, Geophysics, Geosystems*, *12*(1), n/a-n/a. https://doi.org/10.1029/2010GC003230

Heuret, A., Conrad, C. P., Funiciello, F., Lallemand, S., & Sandri, L. (2012). Relation between subduction megathrust earthquakes, trench sediment thickness and upper plate strain. *Geophysical Research Letters*, *39*(5). https://doi.org/10.1029/2011GL050712

Hsu, S.-K., Wu, W.-N., Huang, B.-S., Hsu, Y.-J., Bacolcol, T., & et al. (in press). Recent advances on the tectonics of the Philippine arc-trench system (Springer Atmosphere, Earth, Ocean&Space (AEONS) series).

von Huene, R., & Scholl, D. W. (1991). Observations at convergent margins concerning sediment subduction, subduction erosion, and the growth of continental crust. *Reviews of Geophysics*, *29*(3), 279–316. https://doi.org/10.1029/91RG00969

Jarrard, R. D. (1986). Relations among subduction parameters. *Reviews of Geophysics*, *24*(2), 217–284. https://doi.org/10.1029/RG024i002p00217

Jarrin, P., Nocquet, J.-M., Rolandone, F., Audin, L., Mora-Páez, H., Alvarado, A., et al. (2023). Continental block motion in the Northern Andes from GPS measurements. *Geophysical Journal International*, *235*(2), 1434–1464. https://doi.org/10.1093/gji/ggad294

Kimura, G. (1986). Oblique subduction and collision: Forearc tectonics of the Kuril arc. *Geology*, *14*(5), 404–407. https://doi.org/10.1130/0091-7613(1986)14<404:OSACFT>2.0.CO;2

Kirby, S. H., Stein, S., Okal, E. A., & Rubie, D. C. (1996). Metastable mantle phase transformations and deep earthquakes in subducting oceanic lithosphere. *Reviews of Geophysics*, *34*(2), 261–306. https://doi.org/10.1029/96RG01050

Koulali, A., Susilo, S., McClusky, S., Meilano, I., Cummins, P., Tregoning, P., et al. (2016). Crustal strain partitioning and the associated earthquake hazard in the eastern Sunda-Banda Arc. *Geophysical Research Letters*, *43*(5), 1943–1949. https://doi.org/10.1002/2016GL067941

Koulali, A., McClusky, S., Susilo, S., Leonard, Y., Cummins, P., Tregoning, P., et al. (2017). The kinematics of crustal deformation in Java from GPS observations: Implications for fault slip partitioning. *Earth and Planetary Science Letters*, *458*, 69–79. https://doi.org/10.1016/j.epsl.2016.10.039

Kozhurin, A., & Zelenin, E. (2017). An extending island arc: The case of Kamchatka. *Tectonophysics*, *706–707*, 91–102. https://doi.org/10.1016/j.tecto.2017.04.001

Kozhurin, A., Acocella, V., Kyle, P. R., Lagmay, F. M., Melekestsev, I. V., Ponomareva, V., et al. (2006). Trenching studies of active faults in Kamchatka, eastern Russia: Palaeoseismic, tectonic and hazard implications. *Tectonophysics*, *417*(3–4), 285–304. https://doi.org/10.1016/j.tecto.2006.01.004

Lallemand, S. (2016). Philippine Sea Plate inception, evolution, and consumption with special emphasis on the early stages of Izu-Bonin-Mariana subduction. *Progress in Earth and Planetary Science*, *3*(1), 15. https://doi.org/10.1186/s40645-016-0085-6

Lallemand, S., & Heuret, A. (2017). Subduction Zones Parameters ☆. In *Reference Module in Earth Systems and Environmental Sciences* (p. B9780124095489094951). Elsevier. https://doi.org/10.1016/B978-0-12-409548-9.09495-1

Lallemand, S., Liu, C.-S., Dominguez, S., Schnürle, P., & Malavieille, J. (1999). Trench-parallel stretching and folding of forearc basins and lateral migration of the accretionary wedge in the southern Ryukyus: A case of strain partition caused by oblique convergence. *Tectonics*, *18*(2), 231–247. https://doi.org/10.1029/1998TC900011

Lallemand, S., Heuret, A., & Boutelier, D. (2005). On the relationships between slab dip, back-arc stress, upper plate absolute motion, and crustal nature in subduction zones. *Geochemistry, Geophysics, Geosystems*, *6*(9), 2005GC000917. https://doi.org/10.1029/2005GC000917

Lallemand, S., Heuret, A., Faccenna, C., & Funiciello, F. (2008). Subduction dynamics as revealed by trench migration. *Tectonics*, *27*(3), 2007TC002212. https://doi.org/10.1029/2007TC002212

Lallemand, S., Peyret, M., Arcay, D., & Heuret, A. (2024). Accretion versus erosion and sediment transfer balance near the subduction interface. *Comptes Rendus. Géoscience*, *356*(S2), 27–51. https://doi.org/10.5802/crgeos.252

Lewis, K. B., Lallemand ,Serge E., & and Carter, L. (2004). Collapse in a Quaternary shelf basin off East Cape, New Zealand: Evidence for passage of a subducted seamount inboard of the Ruatoria giant avalanche. *New Zealand Journal of Geology and Geophysics*, *47*(3), 415–429. https://doi.org/10.1080/00288306.2004.9515067

Liu, X., McNally, K. C., & Shen, Z.-K. (1995). Evidence for a role of the downgoing slab in earthquake slip partitioning at oblique subduction zones. *Journal of Geophysical Research: Solid Earth*, *100*(B8), 15351–15372. https://doi.org/10.1029/95JB00870

Mann, P., & Taira, A. (2004). Global tectonic significance of the Solomon Islands and Ontong Java Plateau convergent zone. *Tectonophysics*, *389*(3), 137–190. https://doi.org/10.1016/j.tecto.2003.10.024

Martinez, A., Malavieille, J., Lallemand, S., & Collot, J.-Y. (2002). Strain partitioning in an accretionary wedge, in oblique convergence : analogue modelling. *Bulletin de La Société Géologique de France*, *173*(1), 17–24. https://doi.org/10.2113/173.1.17

Marzocchi, W., Sandri, L., Heuret, A., & Funiciello, F. (2016). Where giant earthquakes may come. *Journal of Geophysical Research: Solid Earth*, *121*(10), 7322–7336. https://doi.org/10.1002/2016JB013054

Mazzotti, S., Dragert, H., Hyndman, R. D., Miller, M. M., & Henton, J. A. (2002). GPS deformation in a region of high crustal seismicity: N. Cascadia forearc. *Earth and Planetary Science Letters*, *198*(1–2), 41–48. https://doi.org/10.1016/S0012-821X(02)00520-4

Mazzotti, S., Dragert, H., Henton, J., Schmidt, M., Hyndman, R., James, T., et al. (2003). Current tectonics of northern Cascadia from a decade of GPS measurements. *Journal of Geophysical Research: Solid Earth*, *108*(B12), 2003JB002653. https://doi.org/10.1029/2003JB002653

McCaffrey, R. (1992). Oblique plate convergence, slip vectors, and forearc deformation. *Journal of Geophysical Research: Solid Earth*, *97*(B6), 8905–8915. https://doi.org/10.1029/92JB00483

McClay, K. R., Whitehouse, P. S., Dooley, T., & Richards, M. (2004). 3D evolution of fold and thrust belts formed by oblique convergence. *Marine and Petroleum Geology*, *21*(7), 857–877. https://doi.org/10.1016/j.marpetgeo.2004.03.009

Nakao, A., Kuwatani, T., Ueki, K., Yoshida, K., Yutani, T., Hino, H., & Akaho, S. (2022). Subduction-zone parameters that control slab behavior at the 660-km discontinuity revealed by logistic regression analysis and model selection. *Frontiers in Earth Science*, *10*. https://doi.org/10.3389/feart.2022.1008058

Nishimura, T. (2011). Back-arc spreading of the northern Izu–Ogasawara (Bonin) Islands arc clarified by GPS data. *Tectonophysics*, *512*(1–4), 60–67. https://doi.org/10.1016/j.tecto.2011.09.022

Nishimura, T., Yokota, Y., Tadokoro, K., & Ochi, T. (2018). Strain partitioning and interplate coupling along the northern margin of the Philippine Sea plate, estimated from Global Navigation Satellite System and Global Positioning System-Acoustic data. *Geosphere*, *14*(2), 535–551. https://doi.org/10.1130/GES01529.1

Patria, A., Tsutsumi, H., & Natawidjaja, D. H. (2021). Active fault mapping in the onshore northern Banda Arc, Indonesia: Implications for active tectonics and seismic potential. *Journal of Asian Earth Sciences*, *218*, 104881. https://doi.org/10.1016/j.jseaes.2021.104881

Patriat, M., Collot, J., Danyushevsky, L., Fabre, M., Meffre, S., Falloon, T., et al. (2015). Propagation of back-arc extension into the arc lithosphere in the southern New Hebrides volcanic arc. *Geochemistry, Geophysics, Geosystems*, *16*(9), 3142–3159. https://doi.org/10.1002/2015GC005717

Perucca, L., Alvarado, P., & Saez, M. (2016). Neotectonics and seismicity in southern Patagonia. *Geological Journal*, *51*(4), 545–559. https://doi.org/10.1002/gj.2649

Petricca, P., & Carminati, E. (2016). Present-day stress field in subduction zones: Insights from 3D viscoelastic models and data. *Tectonophysics*, *667*, 48–62. https://doi.org/10.1016/j.tecto.2015.11.010

Philippon, M., & Corti, G. (2016). Obliquity along plate boundaries. *Tectonophysics*, *693*, 171–182. https://doi.org/10.1016/j.tecto.2016.05.033

Rangin, C., Le Pichon, X., Mazzotti, S., Pubellier, M., Chamot-Rooke, N., Aurelio, M., et al. (1999). Plate convergence measured by GPS across the Sundaland/Philippine Sea Plate deformed boundary: the Philippines and eastern Indonesia. *Geophysical Journal International*, *139*(2), 296–316. https://doi.org/10.1046/j.1365-246x.1999.00969.x

Reilinger, R., McClusky, S., Vernant, P., Lawrence, S., Ergintav, S., Cakmak, R., et al. (2006). GPS constraints on continental deformation in the Africa-Arabia-Eurasia continental collision zone and implications for the dynamics of plate interactions. *Journal of Geophysical Research: Solid Earth*, *111*(B5), 2005JB004051. https://doi.org/10.1029/2005JB004051

Ribeiro, J. M., Stern, R. J., Martinez, F., Ishizuka, O., Merle, S. G., Kelley, K., et al. (2013). Geodynamic evolution of a forearc rift in the southernmost Mariana Arc. *Island Arc*, *22*(4), 453–476. https://doi.org/10.1111/iar.12039

Schellart, W. P. (2008a). Overriding plate shortening and extension above subduction zones: A parametric study to explain formation of the Andes Mountains. *Geological Society of America Bulletin*, *120*(11–12), 1441–1454. https://doi.org/10.1130/B26360.1

Schellart, W. P. (2008b). Subduction zone trench migration: Slab driven or overriding-plate-driven? *Physics of the Earth and Planetary Interiors*, *170*(1–2), 73–88. https://doi.org/10.1016/j.pepi.2008.07.040

Schellart, W. P. (2024). Subduction dynamics and overriding plate deformation. *Earth-Science Reviews*, *253*, 104755. https://doi.org/10.1016/j.earscirev.2024.104755

Schellart, W. P., & Moresi, L. (2013). A new driving mechanism for backarc extension and backarc shortening through slab sinking induced toroidal and poloidal mantle flow: Results from dynamic subduction models with an overriding plate. *Journal of Geophysical Research: Solid Earth*, *118*(6), 3221–3248. https://doi.org/10.1002/jgrb.50173

Scholz, C. H., & Campos, J. (1995). On the mechanism of seismic decoupling and back arc spreading at subduction zones. *Journal of Geophysical Research: Solid Earth*, *100*(B11), 22103–22115. https://doi.org/10.1029/95JB01869

Selvans, M. M., Stock, J. M., DeMets, C., Sanchez, O., & Marquez-Azua, B. (2011). Constraints on Jalisco Block Motion and Tectonics of the Guadalajara Triple Junction from 1998–2001 Campaign GPS Data. *Pure and Applied Geophysics*, *168*(8), 1435–1447. https://doi.org/10.1007/s00024-010-0201-2

Serpelloni, E., Vannucci, G., Pondrelli, S., Argnani, A., Casula, G., Anzidei, M., et al. (2007). Kinematics of the Western Africa-Eurasia plate boundary from focal mechanisms and GPS data. *Geophysical Journal International*, *169*(3), 1180–1200. https://doi.org/10.1111/j.1365-246X.2007.03367.x

Simons, W. J. F., Socquet, A., Vigny, C., Ambrosius, B. a. C., Haji Abu, S., Promthong, C., et al. (2007). A decade of GPS in Southeast Asia: Resolving Sundaland motion and boundaries. *Journal of Geophysical Research: Solid Earth*, *112*(B6). https://doi.org/10.1029/2005JB003868

Socquet, A., Simons, W., Vigny, C., McCaffrey, R., Subarya, C., Sarsito, D., et al. (2006). Microblock rotations and fault coupling in SE Asia triple junction (Sulawesi, Indonesia) from GPS and earthquake slip vector data. *Journal of Geophysical Research: Solid Earth*, *111*(B8). https://doi.org/10.1029/2005JB003963

Stegman, D. R., Freeman, J., Schellart, W. P., Moresi, L., & May, D. (2006). Influence of trench width on subduction hinge retreat rates in 3-D models of slab rollback. *Geochemistry, Geophysics, Geosystems*, *7*(3), 2005GC001056. https://doi.org/10.1029/2005GC001056

Stein, S., & Stein, C. A. (1996). Thermo-mechanical evolution of oceanic lithosphere: Implications for the subduction process and deep earthquakes. *Geophysical Monograph Series*, *96*, 1–17. https://doi.org/10.1029/GM096p0001

Sternai, P., Jolivet, L., Menant, A., & Gerya, T. (2014). Driving the upper plate surface deformation by slab rollback and mantle flow. *Earth and Planetary Science Letters*, *405*, 110–118. https://doi.org/10.1016/j.epsl.2014.08.023

Suárez, R. J., Guillaume, B., Martinod, J., Ghiglione, M. C., Sue, C., & Kermarrec, J.-J. (2022). Role of convergence obliquity and inheritance on sliver tectonics: Insights from 3-D subduction experiments. *Tectonophysics*, *842*, 229583. https://doi.org/10.1016/j.tecto.2022.229583

Symithe, S., Calais, E., de Chabalier, J. B., Robertson, R., & Higgins, M. (2015). Current block motions and strain accumulation on active faults in the Caribbean. *Journal of Geophysical Research: Solid Earth*, *120*(5), 3748–3774. https://doi.org/10.1002/2014JB011779

Turino, V., & Holt, A. F. (2024). Spatio-temporal variability in slab temperature within dynamic 3-D subduction models. *Geophysical Journal International*, *236*(3), 1484–1498. https://doi.org/10.1093/gji/ggad489

Van Keken, P. E., Hacker, B. R., Syracuse, E. M., & Abers, G. A. (2011). Subduction factory: 4. Depth-dependent flux of H_2O from subducting slabs worldwide. *Journal of Geophysical Research*, *116*(B1), B01401. https://doi.org/10.1029/2010JB007922

Vernant, P., Reilinger, R., & McClusky, S. (2014). Geodetic evidence for low coupling on the Hellenic subduction plate interface. *Earth and Planetary Science Letters*, *385*, 122–129. https://doi.org/10.1016/j.epsl.2013.10.018

Villegas-Lanza, J. C., Nocquet, J.-M., Rolandone, F., Vallée, M., Tavera, H., Bondoux, F., et al. (2016). A mixed seismic–aseismic stress release episode in the Andean subduction zone. *Nature Geoscience*, *9*(2), 150–154. https://doi.org/10.1038/ngeo2620

Wallace, L. M., McCaffrey, R., Beavan, J., & Ellis, S. (2005). Rapid microplate rotations and backarc rifting at the transition between collision and subduction. *Geology*, *33*(11), 857. https://doi.org/10.1130/G21834.1

Wallace, L. M., Ellis, S., & Mann, P. (2009). Collisional model for rapid fore-arc block rotations, arc curvature, and episodic back-arc rifting in subduction settings. *Geochemistry, Geophysics, Geosystems*, *10*(5), 2008GC002220. https://doi.org/10.1029/2008GC002220

Wang, K., Hu, Y., Bevis, M., Kendrick, E., Smalley Jr., R., Vargas, R. B., & Lauría, E. (2007). Crustal motion in the zone of the 1960 Chile earthquake: Detangling earthquake-cycle deformation and forearc-sliver translation. *Geochemistry, Geophysics, Geosystems*, *8*(10). https://doi.org/10.1029/2007GC001721

Wang, S., Yu, H., Zhang, Q., & Zhao, Y. (2018). Absolute plate motions relative to deep mantle plumes. *Earth and Planetary Science Letters*, *490*, 88–99. https://doi.org/10.1016/j.epsl.2018.03.021

Wiens, D. A., & Gilbert, H. J. (1996). Effect of slab temperature on deep-earthquake aftershock productivity and magnitude–frequency relations. *Nature*, *384*(6605), 153–156. https://doi.org/10.1038/384153a0

Wirth, E. A., Sahakian, V. J., Wallace, L. M., & Melnick, D. (2022). The occurrence and hazards of great subduction zone earthquakes. *Nature Reviews Earth & Environment*, *3*(2), 125–140. https://doi.org/10.1038/s43017-021-00245-w

Yu, G., Wesnousky, S. G., & Ekström, G. (1993). Slip Partitioning along Major Convergent Plate Boundaries. In *Shallow Subduction Zones: Seismicity, Mechanics and Seismic Potential Part 1* (pp. 183–210). Birkhäuser, Basel. https://doi.org/10.1007/978-3-0348-5846-5_2

Zelst, I. van, Brizzi, S., Rijsingen, E. van, Funiciello, F., & Dinther, Y. van. (2025). Investigating Global Correlations Between Earthquake-generated Tsunamis and Subduction Zone Characteristics. *Τεκτονικα*, *3*(1), 46–63. https://doi.org/10.55575/tektonika2025.3.1.88